Published in final edited form as:

Brain Struct Funct. 2018 September ; 223(7): 3011–3043. doi:10.1007/s00429-018-1678-1.

Two-photon probes for *in vivo* multicolor microscopy of the structure and signals of brain cells

Clément Ricard[1,2,3], **Erica D. Arroyo**[4], **Cynthia X. He**[4], **Carlos Portera-Cailliau**[4,5], **Gabriel Lepousez**[6], **Marco Canepari**[7,8,9], and **Daniel Fiole**[10,11,*]

[1]Brain Physiology Laboratory, CNRS UMR 8118, Paris, F-75006, France

[2]Faculté de Sciences Fondamentales et Biomédicales, Université Paris Descartes, PRES Sorbonne Paris Cité, Paris, F-75006, France

[3]Fédération de Recherche en Neurosciences FR 3636, Paris, F-75006, France

[4]Department of Neurology, David Geffen School of Medicine, University of California, Los Angeles, United States

[5]Department of Neurobiology, David Geffen School of Medicine, University of California, Los Angeles, United States

[6]Unité Perception et Mémoire, Département de Neuroscience, Institut Pasteur, 25 rue du Docteur Roux, F-75724 Paris Cedex 15, France

[7]Laboratory for Interdisciplinary Physics, UMR 5588 CNRS and Université Grenoble Alpes, F-38402 Saint Martin d'Hères, France

[8]Laboratories of Excellence, Ion Channel Science and Therapeutics, France

[9]Institut National de la Santé et Recherche Médicale (INSERM), France

[10]Unité Biothérapies anti-Infectieuses et Immunité, Département des Maladies Infectieuses, Institut de Recherche Biomédicale des Armées, BP 73, F-91223 Brétigny-sur-Orge cedex, France

[11]Human Histopathology and Animal Models, Infection and Epidemiology department, Institut Pasteur, 28 rue du docteur Roux, F-75725 Paris Cedex 15, France

Abstract

Imaging the brain of living laboratory animals at a microscopic scale can be achieved by two-photon microscopy thanks to the high penetrability and low phototoxicity of the excitation

*corresponding author: daniel.fiole@gmail.com.
Current address of DF: CREATIS, CNRS UMR 5220; Inserm U1044; Université de Lyon; Université Lyon 1; INSA-Lyon, 69621 Villeurbanne, France, and: European Synchrotron Radiation Facility, X-ray Imaging Group, 38043 Grenoble cedex, France. Current email address: fiole@esrf.fr.

ORCID iD: CH 0000-0003-1236-3151; CPC 0000-0001-5735-6380; GL 0000-0002-9390-7749; DF 0000-0002-1072-6935.

Compliance with Ethical Standards

Conflict of Interest: GL is supported by the life insurance company AG2R-La-Mondiale ("Vivons vélo pour l'Institut Pasteur").

Ethical approval: All procedures performed in studies involving animals were in accordance with the ethical standards of the institution at which the studies were conducted. This article does not contain any studies with human participants performed by any of the authors.

wavelengths used. However, knowledge of the two-photon spectral properties of the myriad fluorescent probes is generally scarce and, for many, non-existent. Additionally, the use of different measurement units in published reports further hinders the design of a comprehensive imaging experiment.

In this review, we compile and homogenize the two-photon spectral properties of 280 fluorescent probes. We provide practical data, including the wavelengths for optimal two-photon excitation, the peak values of two-photon action cross-section or molecular brightness, and the emission ranges. Beyond the spectroscopic description of these fluorophores, we discuss their binding to biological targets. This specificity allows *in vivo* imaging of cells, their processes, and even organelles and other subcellular structures in the brain. In addition to probes that monitor endogenous cell metabolism, studies of healthy and diseased brain benefit from the specific binding of certain probes to pathology-specific features, ranging from amyloid-β plaques to the autofluorescence of certain antibiotics. A special focus is placed on functional *in vivo* imaging using two-photon probes that sense specific ions or membrane potential, and that may be combined with optogenetic actuators. Being closely linked to their use, we examine the different routes of intravital delivery of these fluorescent probes according to the target. Finally, we discuss different approaches, strategies, and prerequisites for two-photon multicolor experiments in the brains of living laboratory animals.

Keywords

Two-photon cross section; calcium imaging; functional imaging; electroporation; intravital; multicolor microscopy

Introduction

Two-photon excitation fluorescence microscopy, or two-photon microscopy (TPM), became a standard and powerful method of investigation in biology due to its excellent penetrability in living tissues and high spatiotemporal resolution, while inducing low phototoxicity and photobleaching compared to other optical techniques (Denk et al. 1990; So et al. 2000; Zipfel et al. 2003b; Helmchen and Denk 2005). In this review, we focus on neuroscience because the functional and physiological properties of the brain makes it a particularly fecund field for the application of TPM (Svoboda and Yasuda 2006; Mostany et al. 2015).

The sophistication of intravital TPM is currently expanding through three axes: 1. Hardware; 2. Sample preparation and new genetic tools; 3. Fluorescent probes (Crowe and Ellis-Davies 2014). First, as far as hardware there have been improvements and new developments in excitation sources, scanning, and detection. The popularization of optical parametric oscillators (OPO), which allow excitation far beyond the traditional Titanium:Sapphire lasers, helps improve the depth of imaging up to 1.6 mm (Kobat et al. 2011). Deep scattering tissues can be efficiently observed by wavefront optimization thanks to adaptive optics (Ji et al. 2010; Wang et al. 2015). New kinds of detectors like GaAsP photomultipliers or hybrid avalanche photodiodes allow detection of dimmer signals. Also, promising advances in the miniaturization of two-photon microscopes are enabling simultaneous recordings of neural circuit activity in freely moving animals (Yu et al. 2015; Zong et al. 2017) while avoiding

the side effects associated with the use of anesthetics (Tran and Gordon 2015; Santisakultarm et al. 2016).

Second, refinements in sample preparation beyond the original glass-covered cranial windows (Holtmaat et al. 2009) and skull thinning (Yang et al. 2010) now permit chronic live imaging below the superficial layers of neocortex. For example, a substantial increase in resolution can be achieved by replacing the single coverslip with a pair of coverslips separated by a thin layer of air, which minimizes the effects of spherical aberration (Estrada et al. 2015). Also, surgical GRIN lens implantation can be combined with head-mounted miniscopes (Resendez et al. 2016) or standard two-photon microscopes for imaging of deep brain structures such as hippocampus (Crowe and Ellis-Davies 2014).

In vivo TPM imaging also benefits from the use of genetic tools that can target fluorochrome expression to different brain cells, including promoters for specific cell types (*e.g.*, Thy1 mice for Layer 5B neurons (Feng et al. 2000), CX3CR1 mice for microglia (Jung et al. 2000)). Cre-Lox recombination can be fruitfully used to target any fluorescent protein in spatially restricted patterns, such as different cell types, cortical layers, or brain regions, thanks to the existence of a number of Cre driver lines. Other genetic strategies (*e.g.*, Cre-ER^{T2}) can temporally restrict expression (Kristianto et al. 2017). Different fluorochromes can be simultaneously expressed on different cells of the same lineage thus (*e.g.*, the Brainbow construct (Livet et al. 2007)) or on different cell types by breeding together mice of different phenotypes (*e.g.*, Thy1-**CFP**/LysM-**GFP**/CD11c-**EYFP** (Fenrich et al. 2013)).

Designing new transgenic animal models has been recently made less arduous than previously by CRISPR/Cas9 (Wang and Qi 2016) and PiggyBac (Woodard and Wilson 2015) technologies, but remains a time-consuming task that can be overcome by the administration of exogenous fluorescent probes. Depending on the target and on physical and chemical properties of the probe, methods of administration can range from intravenous dye injection to *in utero* electroporation and viral protein transduction.

Third, the availability of increasing numbers of two-photon-suitable synthetic dyes or genetically encoded probes with extended properties has brought new perspectives to the use of TPM in neuroscience. One of these perspectives consists of two-photon functional imaging, which makes possible to witness brain cells ‘at work’ thanks to voltage-sensitive dyes, probes that monitor levels of various ions (*e.g.*, Cl^{-}, Ca^{2+}) (Helmchen 2009), or caged neurotransmitters that can be photoreleased with TPM (Hess et al. 2014).

Beyond the prolific engineering of new fluorescent proteins that unquestionably and fruitfully expands the biological applications of TPM (Pak et al. 2015), its routine use is hindered by the need for a more extensive characterization of spectral properties of existing fluorescent probes. Recent developments in far-red two-photon excitation make the need for an update of the spectral characteristics of fluorescent probes even more acute (Herz et al. 2010; Mojzisova and Vermot 2011). While commercial and academic databases of one-photon absorption spectra are well documented, the two-photon specifications of most probes are only scarcely documented, despite a small number of helpful initiatives (Bestvater et al. 2002; Cahalan et al. 2002; Drobizhev et al. 2011; Mütze et al. 2012;

Romanelli et al. 2013; Lim and Cho 2013). In this review, we provide a comprehensive list of two-photon–related spectral and biological properties of more than 280 fluorescent probes, and discuss different routes of delivery of such probes into laboratory animals, as well as their actual or prospective relevance to *in vivo* multicolor TPM of cells, structures, and functions, in the healthy and diseased brain.

1) Reaching the target

1.1 Intravenous route—Blood vessels transport oxygen and nutriments in the whole organism and can be used to deliver fluorescent dyes into the tiniest parts of an organ (*cf.* Table 1).

Blood vessel labeling requires only the intravenous delivery of a fluorescent dye to efficiently stain an entire organ's vascular tree, which can then be observed *in vivo* with TPM by a z- stack acquisition (Tozer et al. 2005; Ricard et al. 2013b). Common dyes such as **fluorescein** or **rhodamine** (*cf.* Table 2) can be used; these are harmless to the animal and cleared from the circulation after a few hours. As capillaries can be permeable to small molecules, these dyes are usually conjugated with a large molecular weight dextran that is too large to leak into the tissue. The molecular weight of the resulting dye can thus be chosen depending on the permeability of the targeted type of vessel. Neocortical arteries and arterioles can be specifically labeled using **Alexa Fluor 633** (*cf.* Table 3), which binds to elastin fibres (Shen et al. 2012). However, when multicolor labeling is required, green or red channels are frequently chosen through the use of other fluorophores or fluorescent proteins (*e.g.*, **EGFP** or **DsRed).** Blue-emitting dyes such as **Cascade Blue** have been successfully used in intravital studies and can efficiently be excited by TPM (Ricard and Debarbieux 2014; Ricard et al. 2016b). It must be considered, however, that in living tissues the maximum imaging depth is a function of the wavelengths of both the excitation and fluorescence beam. In the TPM range, high-energy photons are quickly absorbed by the tissue, resulting in a reduced imaging depth (König 2000). Such a parameter has to be taken into account in the design of the experiment. Moreover, fluorescent dyes conjugated to dextrans can be captured by phagocytes resulting in a long-lasting labeling of these cells (Fenrich et al. 2012; Fiole et al. 2014). Such labeling is observed in the brain and spinal cord dura mater for several days after a single intravenous injection and can impede the correct segmentation of blood vessels during image processing. **Quantum dots** were introduced as an alternative to classic fluorescent dyes. They present low toxicity, are not engulfed by macrophages, have reduced photobleaching, and can fluoresce in the red and deep-red range, making them particularly suitable for multicolor imaging (Mashinchian et al. 2014). It was also demonstrated that excitation of quantum dots using an optical parametric oscillator can improve imaging depth of vasculature in the brain and the spinal cord (Kobat et al. 2009, 2011; Ricard et al. 2016a). The fluorescence intermittency of quantum dots (Frantsuzov et al. 2013) should however be taken into consideration especially for single-particle tracking, unless their nonblinking properties are established (Marchuk et al. 2012; Lane et al. 2014).

Intravenous injections of fluorescent dyes have also been used to label other structures. **Sulforhodamine 101** and **Sulforhodamine B** were reported to leak out of the vasculature and to stain specifically astrocytes (*cf.* Table 1 and Table 3) without showing adverse

reactions on astrocytic calcium signals or electroencephalographic recording *in vivo* (Appaix et al. 2012; Vérant et al. 2013). **Sulforhodamine B** was also demonstrated to stain elastic fibers in blood vessel walls, as well as in muscles after a single intravenous injection (Ricard et al. 2007). Intravenous injection of fluorescent probes can also be used to determine the acidity of tissues using pH indicators (*cf.* Table 4), or to measure physiological parameters such as cerebral blood flow (Chaigneau et al. 2003) and blood-brain-barrier permeability (Ricard et al. 2009) in different pathologies, including vascular occlusion (Schaffer et al. 2006) and brain tumors (Ricard et al. 2013b, 2016b). Investigating the properties of the blood vessel tree enables the assessment of side effects of treatments in preclinical trials (Ricard et al. 2013a). For instance, the blood vessel density of glioblastoma-animals injected with **Rhodamine B** dextran was recorded over time. Experiments conducted in untreated conditions and after the administration of bevacizumab, an anti-angiogenic compound, revealed a lack of correlation between tumor growth and blood vessel density (Ricard et al. 2013b).

As an alternative but comparable route to intravenous delivery, intraperitoneal administration (*cf.* Table 1) of fluorochromes can also be performed to stain structures in the diseased brain (*cf.* Table 5). For example, in Alzheimer's disease research, amyloid-β plaques can be specifically stained by intraperitoneal administration of **SAD1** (Heo et al. 2013) or **Methoxy-X04** (Klunk et al. 2002), revealing the kinetics of amyloid-β plaques growing over months (Burgold et al. 2011).

1.2 Whole-cell and bulk loading—A large population of neurons can be bulk-loaded with a cell membrane-permeable acetoxymethyl (AM) ester-conjugated indicator form (*e.g.*, **Fura-2-AM** or **Fluo-4-AM**) (Garaschuk et al. 2006; Brenowitz and Regehr 2014) or dextran-conjugated form, enabling readout of activity across a network (Yuste et al. 2011; Reeves et al. 2011). Bulk-loading of ion indicators may be spatially restricted to the soma and most proximal processes of neural cells. However, Reeves *et al.* have shown that performing morphological reconstructions after bulk-loading of astrocytes in the CA1 region of the hippocampus from rats can help detecting calcium transients in distal astrocyte processes (Reeves et al. 2011).

Alternatively, chemical ion indicators can be typically delivered into single cells via micropipettes (enabling electrophysiology) or electroporation (Liu and Haas 2011; Grienberger and Konnerth 2012). While the chemical indicators have high sensitivity and fast on-off kinetics allowing for precise temporal resolution of action potentials, they are typically used in acute experimental preparations (a few hours at most), and they are not amenable for labeling of specific cell populations (Grienberger and Konnerth 2012).

1.3 Viral transduction—In order to allow expression of new genes coding for fluorescent proteins in spatially-restricted and genetically-defined neurons, researchers have developed a versatile toolbox of replication-incompetent recombinant viral vectors (*cf.* Table 1) that are devoid of most of their natural genetic material and loaded with engineered constructs (Nassi et al. 2015). The diversity of available vectors reflects the different specifications of each viral vectors in terms of:

1. tropism for cell type, compartment (axonal *vs.* somato-dendritic), and animal species. This tropism is directly influenced by the nature of the glycoprotein of the envelope (which defines the serotype) and the expression of receptors for envelope glycoprotein on targeted cells leading to vector internalization;
2. transduction and expression efficiency, speed of expression after infection, and stability for long term expression;
3. vector genome size and maximum insert size, ease of manipulating the genome and producing high-titer solutions, and integration into the host genome;
4. and immunogenicity, cell toxicity and safety.

Here we list the main viral vectors used in the neuroscience field and their general features:

- retroviruses are integrative vectors with an insert size up to 8-9 kB, providing a stable long-term expression. They exclusively transduce dividing cells and show moderate immunogeneticity.
- lentiviruses are integrative vectors with an insert size up to 8-9 kb, good for stable long-term expression. They have a large tropism and can transduce most CNS cells (astrocytes, neurons, and oligodendrocytes) and show moderate immunogeneticity.
- adeno-associated viruses (AAV) are currently the most commonly used vector for gene delivery. They are non-integrative vectors with an insert size up to 4-5 kb. Because of their small size and high titer production, a single injection can infect a large volume of tissue. They are also favored over other vectors for their mild immunogenicity and a dominant neuronal tropism. To enlarge their tropism, envelope proteins have been engineered using directed evolution to target specific cell types (*e.g.*, oligodendrocytes (Büning et al. 2015; Powell et al. 2016)) or to target specific neuronal compartments (*e.g.*, axonal domain for retrograde labeling of neurons (Tervo et al. 2016)).
- Herpes Simplex Virus (HSV-1) is a non-integrative vector with an insert size up to 100 kb. Although its complex genome is not easy to manipulate, HSV-1s transduce mainly neurons with a dominant axonal tropism, making them an interesting tool for retrograde labeling of neurons. Importantly, they show significant immunogenicity and cell toxicity.
- Canine Adenovirus (CAV-2) is a non-integrative vector with a smaller insert size up to 30 kb (Junyent and Kremer 2015). CAV-2s transduce mainly neurons with a dominant axonal tropism, making them an interesting tool for retrograde labeling of neurons. The main receptor for the internalization of the virus is the coxsackievirus and adenovirus receptor (CAR). They also show a significant immunogenicity and cell toxicity.
- Rabies virus (RABV) is a non-integrative vector with an insert size of 4-5 kb. RABVs are neurotropic and are classically used as replication-conditional pseudotyped viruses for retrograde tracing of mono-synaptic inputs onto genetically-defined cell populations (Wickersham et al. 2007). Rabies virus is

pseudotyped with the EnVA glycoprotein to ensure that the virus exclusively infects cells expressing the EnvA receptor (TVA). The virus also lacks the envelope glycoprotein and expresses the gene of interest. Complementation of the modified rabies virus with the envelope glycoprotein in the TVA-expressing cells allows the generation of infectious particles, which trans-synaptically infect presynaptic neurons. Importantly, rabies virus shows strong neurotoxicity with longer-term infection (>15 days).

1.4 *In utero* electroporation—*In utero* electroporation (IUE) is a technique that enables researchers to express genes of interest within specific neuronal populations (*cf.* Table 1) by targeting plasmid DNA constructs directly to the embryonic brain of rodents (Fukuchi-Shimogori and Grove 2001; Saito and Nakatsuji 2001; Takahashi et al. 2002; Wang and Mei 2013). Although this section focuses on cerebral cortex, IUE can be used for gene transfer in other brain regions (Takiguchi-Hayashi et al. 2004; Borrell et al. 2005; Nakahira et al. 2006; Navarro-Quiroga et al. 2007; Bonnin et al. 2007). For cortical labeling, IUE takes advantage of one of the most reliable and tightly regulated processes that occurs during brain development: the sequential inside-out laminar organization of the cortex, whereby neurons in deeper layers are generated before those in more superficial layers (Angevine and Sidman 1961; Rakic 1974). IUE is performed at the gestational age that coincides with the generation of pyramidal precursor cells at the subventricular zone along the lateral ventricles. These newborn neurons eventually migrate to and incorporate into their appropriate cortical layer (Caviness and Takahashi 1995; Tabata and Nakajima 2001). For instance, to label layer 2/3 excitatory pyramidal neurons, IUE is performed at embryonic day (E)15-16 (Saito and Nakatsuji 2001).

Although IUE can be used to over-express essentially any protein of interest, it is perhaps most often used to express fluorescent proteins that make it possible to image neuronal structure with confocal or two-photon microscopy. Because IUE can provide sparse labeling in neurons, it is particularly well-suited for high-resolution imaging of the finest detail of neuronal structure, such as dendritic spines. Another major advantage of IUE over traditional fluorescence labeling techniques such as transgenic mouse lines, is that it enables researchers to conduct early postnatal imaging. This is due to the fact that expression of fluorescent proteins (*e.g.*, **GFP**, **YFP**) in transgenic mouse lines is often driven by promoters that initiate transcription after synaptogenesis has already been completed in neocortex; for example, cortical expression of **YFP** in Thy1-eYFP-H mice occurs around postnatal day (P) 21 (Feng et al. 2000; Porrero et al. 2010)). IUE can also achieve potent transduction of fluorescent proteins through the use of constitutively active promoters such as pCAG or other CMV variations (Saito and Nakatsuji 2001); this is particularly useful for deep tissue imaging with *in vivo* TPM. Following IUE, mice can be imaged from perinatal development through adulthood (Cruz-Martin et al. 2010). Another problem with transgenic lines is that layer specificity is limited by the fidelity of the promoter itself and specific Cre lines are not yet available for desired cell types or brain regions, or they may have off target expression. In contrast, IUE at different embryonic stages can be used to target different cortical layers in different locations. Furthermore, tailoring DNA plasmid constructs to a particular experimental design is less expensive and less time-consuming than generating new mouse

lines. Additionally, co-labeling cells with multiple fluorophores using IUE can easily be achieved by co-injecting multiple plasmids or by using bi-cistronic promoters (*e.g.*, P2A (Kim et al. 2011)). It is also possible to design plasmids to express opsins or DREADD constructs, to genetically manipulate subpopulations of neurons both constitutively and conditionally (Takahashi et al. 2002; Matsuda and Cepko 2004, 2007; Yasuda et al. 2006; Huber et al. 2008; Manent et al. 2009). IUE also affords significant flexibility because the level of expression can be controlled by varying the voltage delivery, concentration of the plasmid, and the volume injected. Of note, IUE may not be compatible with the expression of fluorescent calcium indicators (**GCaMP6**) as anecdotal reports suggest that few if any neurons survive postnatally, presumably due to some toxicity from calcium buffering. In conclusion, IUE is a powerful method for the expression of proteins in the early postnatal brain and into adulthood, especially for layer-specific cortical neurons.

2) Interrogating neural signals

2.1 Calcium imaging—The ability to measure changes in ion levels in living tissues with fluorescent microscopy offers many possibilities for scientific investigations (*cf.* Table 6). Across cell types and within multiple intracellular compartments, calcium ions (Ca^{2+}) play a variety of important roles, including cell cycle regulation, gene transcription modulation, intracellular signaling, muscle contraction and neurotransmission (Grienberger and Konnerth 2012). Action potentials in neurons result in massive influxes of Ca^{2+} through voltage-gated channels, as well as the release of Ca^{2+} from intracellular stores (Kandel et al. 2000), and fluctuations in free Ca^{2+} in the presynaptic and postsynaptic compartments contribute to activity-dependent plasticity (Grienberger and Konnerth 2012). Because changes in the level of intracellular Ca^{2+} are a robust indicator of action potential firing in neurons, fluorescent Ca^{2+} indicators have become powerful tools for recording neural activity with excellent spatial and temporal resolution. Additionally, different types of Ca^{2+} signaling events have been studied in astrocytes (Srinivasan et al. 2015) and in cardiomyocytes (Herron et al. 2012).

In general, Ca^{2+} imaging relies on a fluorescent sensor compound that is introduced into neurons (or other cells) and that, when bound to Ca^{2+}, changes its fluorescent properties. The two primary classes of Ca^{2+} indicators are the synthetic chemical indicators and the genetically encoded indicators. The chemical calcium indicators (*e.g.*, **Fura-2**, **Indo-1**, **Fluo-4**, **Oregon Green BAPTA-1**) were pioneered by Roger Tsien's group and utilize a synthetic Ca^{2+} chelator combined with a fluorophore (Grynkiewicz et al. 1985; Tsien et al. 1985; Brain and Bennett 1997; Gee et al. 2000). When Ca^{2+} binds to the chelator site, the molecule undergoes a conformational change that alters the spectrum of emitted fluorescence (Grienberger and Konnerth 2012). **Fura-2** is excited by ultraviolet wavelengths, produces peak fluorescence at 505-520 nm, and has relatively fast kinetics (Tsien et al. 1985). Under two-photon excitation, **Fura-2** fluorescence decreases as [Ca^{2+}] increases, producing decreases in fluorescence intensity during neuronal activity. In contrast, the fluorescence emitted by **Fluo-4** and **Oregon Green BAPTA-1** increases above its baseline as [Ca^{2+}] increases during action potential firing.

The genetically encoded Ca^{2+} indicators (GECIs) use a Ca^{2+} binding protein, such as calmodulin or troponin, instead of a chelator like BAPTA. Since the discovery of the green fluorescent protein, scientists have generated an array of sensors combining **GFP** variants with Ca^{2+}-binding proteins. The GECI subcategory of cameleons (Miyawaki et al. 1997), is perhaps the most popular amongst GECIs, but other varieties exist based on troponin-C as the Ca^{2+}-binding protein (Mank et al. 2008). Yellow Cameleon (Nagai et al. 2004) utilizes Förster resonance energy transfer (FRET) between two different fluorescent proteins, linked by calmodulin and calmodulin binding peptide M13. Upon calmodulin binding to Ca^{2+}, the conformational change brings the two fluorophores – one **ECFP** and one **Venus-YFP** – close enough to result in activation of the yellow, resulting in a measurable change in the cyan:yellow fluorescence ratio (Nagai et al. 2004; Grienberger et al. 2014).

For *in vivo* two-photon Ca^{2+} imaging, the most frequently used GECI is the cameleon-based **GCaMP** variety, which utilizes a single circularly permuted green fluorophore (**GFP**) attached to calmodulin and the M13 peptide, and is maintained in a low fluorescence state when Ca^{2+} is not bound (Nakai et al. 2001). Ca^{2+} binding to calmodulin causes a conformational shift that changes the solvent exposure of the **GFP** and allows a fluorescence increase (Chen et al. 2013). Earlier versions of **GCaMP** indicators had relatively low slow on-off kinetics and signal-to-noise ratio, which could however be improved by 3D Block-Matching filtering (Danielyan et al. 2014). More recently, the development of the "ultrasensitive" **GCaMP6** has improved neuronal event detection capability to single-spike resolution, though the off-kinetics remain somewhat slow (Chen et al. 2013). Typical expression methods for GECIs include viral transduction (Chen et al. 2013), with the associated limitation of eventual cytotoxicity caused by long-term calcium sequestration; and transgenic mice expressing **GCaMP** (Zariwala et al. 2012; Chen et al. 2012; Dana et al. 2014). Finally, it is important to note that continual improvements have also been made in red-shifted GECIs (Looger and Griesbeck 2011), with the most recent iterations being **jRCaMP1a**, **jRCaMP1b**, and **jRGECO1a** (Dana et al. 2016). Further developments in these latter GECIs will allow neuroscientists to record from even deeper brain structures, due to the reduced scattering of longer-wavelength excitation light.

2.2 Sodium imaging—Another important ion that can be measured intracellularly is Na^+. In contrast to Ca^{2+} indicators, Na^+ indicators are designed to measure Na^+ concentration in millimolar ranges and therefore these dyes have significantly lower affinity. A commonly used indicator is **SBFI** that is excitable in the UV range and has ratiometric properties similar to **Fura** indicators. This indicator has been used to measure Na^+ in neurons (Myoga et al. 2009) and astrocytes (Langer and Rose 2009). An alternative indicator excitable with blue light is **Sodium Green** that was also used to measure Na^+ in neurons (Senatorov et al. 2000). More recently, a greater sensitivity for fast Na^+ changes in neuronal axons was found for the green excitable indicator **ANG-2** (Miyazaki and Ross 2015).

2.3 Voltage-sensitive dyes—One problem with Ca^{2+} imaging is that the kinetics of the dyes, on the order of hundreds of milliseconds or seconds, are orders of magnitude slower than the duration of typical action potentials. As a result, one cannot record neural activity with precise temporal resolution, which is critical for phenomena like spike timing

dependent plasticity. Ideally, one would want to record changes in membrane potential (V_m), using either organic (*cf.* Table 6) or genetically encoded voltage sensors (GEVS), which have exquisite temporal resolution. *In vivo* voltage-sensitive dye (VSD) imaging from large cell populations in the anesthetized mammalian brain was developed in the nineties (Shoham et al. 1999; Petersen et al. 2003; Grinvald and Hildesheim 2004). This approach is sometimes coupled with intracortical microstimulation and electrode recordings, and requires either injection or topical application (Murphy et al. 2008) of oxonol VSDs, such as **RH-1692**. These have been designed to absorb light in the red region and are therefore outside the absorption band of haemoglobin (which causes pulsation and hemodynamic noise in brain recordings). More recently, styryl VSDs with similar spectral properties were developed (Zhou et al. 2007). The techniques of *in vivo* VSD imaging from large cell populations, using oxonols dyes, further progressed until enabling recordings from the barrel cortex of awake head-fixed mice (Poulet and Petersen 2008) or from freely moving animals (Ferezou et al. 2006).

Among the other *in vivo* applications of VSD imaging, it is important to mention the studies on embryonic developing nervous systems (Kamino et al. 1989). For this application, absorption VSDs such as NK2429 (Fujii et al. 1981) are typically used, since the high translucency of embryonic tissue allows high-sensitivity absorption measurements (Momose-Sato et al. 2001). To achieve *in vivo* V_m imaging with cellular or subcellular resolution, two-photon excitation can be used. To this purpose, the two-photon cross-sections of several styryl VSDs were measured (Fisher et al. 2005). Action potentials from mammalian nerve terminals were then recorded in an *ex vivo* preparation, the neurohypophysis (*pars nervosa*), using the VSD **di-3-ANEPPDHQ** (Fisher et al. 2008). More recently, some novel fluorinated VSDs (Yan et al. 2012) that appear to be more photostable when excited by two photon were developed, and have been used to resolve action potentials from dendritic spines in brain slices (Acker et al. 2011).

In many cases, *in vivo* two-photon V_m imaging requires the topical application of two-photon suitable VSD (*cf.* Table 1) after craniotomy (Murphy et al. 2008). This challenging approach is highly rewarding as it allows V_m imaging during wakefulness after topical administration of **ANNINE-6** (Kuhn et al. 2008), opening the door for simultaneous V_m imaging and behavioral tests.

In summary, *in vivo* V_m imaging using organic indicators has several practical limitations associated with dye loading, access to small structures, and stability of recordings. Most of these limitations can be however overcome by replacing organic indicators with GEVS that can be expressed *in vivo* by viral transduction (Marshall et al. 2016). The first generation of GEVS was developed by mutating the *Drosophila* Shaker potassium channel and fusing it to a **GFP** protein (Siegel and Isacoff 1997). While good optical responses to V_m changes could be obtained by expressing the sensor in oocytes, the protein could not be expressed in the plasma membrane of mammalian neurons and therefore a second generation of GEVS was developed (Dimitrov et al. 2007). These GEVSs, now expressed in neuronal outer membranes, were based on the voltage-sensitive phosphatase from the sea squirt, *Ciona intestinalis*, fused to a **CFP** and **YFP** FRET pair (Lundby et al. 2008). From these pioneering works, new GEVS based either on single FRET pairs (Jin et al. 2012) or on **GFP**

probes (St-Pierre et al. 2014) have been more recently developed with faster responses and enhanced sensitivity, opening the gate to future explorations of activity in the living brain.

2.4 Optogenetics actuators—Optogenetic technology has become an essential tool to study the structure and the function of the neural circuits underlying behavior and cognition. Using photosensitive microbial opsin genes expressed into genetically defined neurons, optogenetics provides millisecond-precision control —activation or inhibition — of defined circuit elements in intact organisms with light (reviewed by Deisseroth (Deisseroth 2015)). Recent developments have provided a large diversity of excitatory and inhibitory opsins that are sensitive to different wavelengths. For instance, red-light-activated opsins (such as C1V1, ChRimson) allow simultaneous activation of neurons and imaging of neuronal activity with the green genetic probe **GCaMP**. Optogenetic tools have been upgraded to achieve two-photon manipulation of neuronal populations at the single-cell resolution. The red-light-activated C1V1 opsin allows the robust generation of precise and fast spike trains using 1,040-nm light and standard raster-scanning light delivery (Prakash et al. 2012). This tool can also be used in combination with two-photon imaging of **GCaMP** probe using 920-nm light (Rickgauer et al. 2014; Packer et al. 2015). Inhibitory opsins such as eNpHR3.0 have also proven to be efficient for neuronal inhibition using 1,040 nm light (Prakash et al. 2012). New illumination methods now exist to improve opsin activation, such as spiral scanning, temporal focusing and holography-based patterned light illumination (Papagiakoumou et al. 2013). Thus, combining optogenetics with imaging technologies opens new avenues to all-optical interrogation of neuronal circuits with closed-loop manipulation of neurons in real time (Emiliani et al. 2015).

2.5 Spectral properties of endogenous molecules—Utilizing the intrinsic spectral properties of the target tissue, when possible, places the experimenter in a very favorable situation by avoiding the complicated, invasive, and/or possibly bias-inducing administration and binding of exogenous fluorescent probes.

Many, if not all endogenous molecules display a certain capacity of two-photon excitation, though this excitation is generally rather inefficient. What appears in most cases to produce an annoying background noise does carry some meaningful information. The two-photon action cross-section spectra of several intrinsic molecules (among which **NADH**, **riboflavin**, **folic acid**, **cholecalciferol**, **pyridoxine**, and **retinol**) has been assessed in the early 2000s by the laboratory of Watt W. Webb at Cornell (Zipfel et al. 2003a), facilitating the two-photon–based analysis of metabolism (*cf.* Table 7). Investigating cell dysfunction in a number of pathologies is made possible through the measurement of the fluorescence decay using fluorescence lifetime imaging (FLIM) of metabolites. For instance, **NADH** FLIM-experiments allowed a better characterization of tumor-associated microglia phenotypes (Bayerl et al. 2016), unveiled the role of astrocytes in chronic neuroinflammation-related neuronal death (Mossakowski et al. 2015; Radbruch et al. 2016), and provided a label-free and non-invasive mean to identify neuron- or glial- biased progenitors (Stringari et al. 2012). Moreover, simultaneous FLIM-based detection of several metabolites like **NADH** and **FAD** with SHG can be achieved through wavelength mixing (Stringari et al. 2017) (for more details, see section *Designing a microscopy setup for intravital multicolor TPM*).

Although not endogenous, it is worth mentioning the very few instances of therapeutic agents whose two-photon spectral characteristics are known: the fluoroquinolone antibiotics **gatifloxacin** and **moxifloxacin** (Lee et al. 2016) (*cf.* Table 5), and **quinacrine** (Bestvater et al. 2002) which stains nucleic acids (*cf.* Table 8) while having several therapeutic indications (Wallace 1989; Eriksson et al. 2015; Lippes 2015).

3) Combining fluorescent probes for multicolor TPM

3.1 Designing a multicolor animal model—The first point to consider when designing an intravital multicolor TPM experiment is the co-labeling of multiple targets in the biological sample. Such labeling can result from crossing transgenic mice that express fluorescent proteins in different cells or structures of interest. For instance, triple transgenic fluorescent mice were described and successfully involved in intravital multicolor TPM experiments (Fenrich et al. 2013; Ricard and Debarbieux 2014). However, producing such animals requires many crossings that considerably delay their use and increase the cost of the experiment. Another approach to multicolor imaging is the Brainbow transgenic mouse, which takes advantage of Cre/lox recombination to stochastically express different fluorescent proteins in a cell population. As a consequence, each cell randomly express a combination of fluorescent proteins and thus can be followed individually (Livet et al. 2007; Weissman and Pan 2015). Different probes can be used to highlight structures and/or functions (*e.g.*, VSD or calcium-sensitive dyes) (Akemann et al. 2013; Shigetomi et al. 2013, 2016; Xu et al. 2017).

Taking advantage of the intrinsic properties of endogenous molecules is an elegant way to investigate biological tissues without the drawbacks associated with the administration, binding and possibly metabolization of exogenous molecules. Second-harmonic generation (SHG) can be used to visualize not only the meninges via type-I or –III collagen imaging (Williams et al. 2005; Ricard et al. 2007; Keikhosravi et al. 2014; Ricard and Debarbieux 2014), but also membrane potential (Rama et al. 2010; Loew and Lewis 2015). Third-harmonic generation (THG) highlights water-lipids and water-proteins interfaces (Débarre et al. 2006; Weigelin et al. 2016) and was successfully tested *in vivo* to image neurons, white-matter structures, and blood vessels simultaneously (Witte et al. 2011). Both SHG and THG require no staining at all and are observed at half or one-third of the excitation wavelength respectively. Beside the respective specificity of SHG and THG, they have been fruitfully used to record morphological landmarks and help data registration during longitudinal *in vivo* imaging of neural zebrafish stem cells (Dray et al. 2015). Autofluorescence does arise from molecules and structures under specific excitation wavelengths (Zipfel et al. 2003a; Ricard et al. 2012). At best autofluorescence may carry relevant information, and at worst, being aware of it may help achieve higher contrast between the background and structures of interest by choosing fluorophores accordingly. It must be noted that autofluorescence signals are not very bright in intravital conditions (*cf.* Table 7) and were mainly described in explants or tissue slices. Due to the low intensity of endogenous signals, one could be tempted to increase the laser power. However, this usually causes artifacts to appear, whose monitoring can help in evaluating photodamage induced during the experiment (Galli et al. 2014).

The preparation of a biological sample for intravital multicolor TPM often requires combining different approaches to label a maximal number of structures of interest involved in a complex process. For example, using Thy1-**CFP**/LysM-**GFP**/CD11c-**EYFP** triple transgenic mice intravenously injected with **Rhodamine B** dextran or Quantum-dots 655, Fenrich *et al.* have revealed a differential spatiotemporal recruitment of myelomonocytic cells after a spinal cord injury (Fenrich et al. 2013). Recently, Ricard *et al.* have described the combination of a LysM-**EGFP**/CD11c-**EYFP** mouse implanted with **DsRed**-expressing glioblastoma cells and intravenously injected with **Cascade Blue** dextran in order to study the recruitment of immune cells during glioblastoma progression (Ricard et al. 2016b).

The development of the co-staining protocol of a biological sample to be used for intravital multicolor TPM must follow some guidelines:

1. Spectral overlap of the emission spectra of all of the utilized fluorophores must be minimal,
2. Utilized fluorophores must not bias physiological and biological properties of the sample nor the pathological condition that is observed,
3. As multiple-fluorophore-expressing animals are difficult to produce, the experimental design should take into account the risk of a downsized animal cohort.

3.2 Designing a microscopy setup for intravital multicolor TPM—The next point to consider, when multicolor TPM is required for an experiment, is the microscopy setup (*cf.* Figure 1). Excitation spectra of the fluorophores are the first elements to take into account. The majority of blue-, green- and red-emitting fluorophores can be excited with a Ti:Sapphire femtosecond laser, as its emission wavelength is generally tunable in between 700 and 1,040 nm. When the excitation spectra of different fluorophores overlap, it is advisable to use a single excitation wavelength (for example, 1000 nm to excite both **Cal-590** and **Oregon Green Bapta-1** (Tischbirek et al. 2015) while they are optimally excited at respectively λ_{ex} = 1050 nm and λ_{ex} = 800 nm) and tune precisely the gain of detectors associated with each fluorophore. The laser power should be kept as low as possible and the experiment duration as short as possible, to limit photobleaching and phototoxicity. This is essential for multicolor timelapse experiments (Fenrich et al. 2013; Ricard et al. 2016b), in which the same region is scanned over and over, at the risk of exposing the tissue to an energy that would threaten its health and/or integrity. When different excitation wavelengths are required (for example, when both **Cascade Blue** with λ_{ex} = 800 nm and **eGFP** with λ_{ex} = 940 nm are present in the same biological sample), a sequential acquisition or the simultaneous use of two Ti:Sapphire femtosecond lasers is required. Continuous sequential acquisition (for example, for calcium imaging recordings) increases the total acquisition time of the images, which is of concern as far as preventing photodamage and prolonged exposure of the animal to anesthetics (if applicable), or depending on the characteristic time of the studied phenomenon.

Deep-red fluorophores require higher excitation wavelengths that cannot be delivered by Ti:Sapphire femtosecond lasers alone. Typically, they are excited by Ytterbium lasers (1,040

nm) but the addition of an OPO (Herz et al. 2010) pumped by a Ti:Sapphire femtosecond laser can enable excitation wavelengths ranging from 1,050 to 1,300 nm when pumped at 800 nm. Simultaneous utilization of both a Ti:Sapphire femtosecond laser and an OPO is achievable. Interestingly, it enables the simultaneous two-photon excitation of three fluorophores with distinct absorption spectra insofar as the pulses of the laser and OPO are synchronized. The excitation of the three fluorophores is done by the femtosecond laser, the OPO and by their spatiotemporal overlap that produces a third two-photon excitation. With such a wavelength mixing, **CFP**, **YFP** and **tdTomato** – having distinct two-photon absorption spectra – can be simultaneously excited. Biological phenomena such as cell movements in embryonic tissues were thereby monitored over time using Brainbow constructs (Mahou et al. 2012). Endogenous metabolites such as **NADH** and **FAD** can also be detected by FLIM, simultaneously with the SHG of surrounding tissues, using a wavelength mixing approach (Stringari et al. 2017). In this case, two-photon excitations are produced by the synchronization of two excitation beams at 760 nm (**NADH** and **FAD**) and 1041 nm that creates a third (virtual) wavelength at 879 nm (**FAD**) (*cf.* Figure 2).

More recently, the efficient detection of up to 7 tissue compartments (five fluorophores, SHG from collagen, and autofluorescence) has been reported using wavelength mixing combined with both a broad set of fluorophores (*cf.* Figure 3) and a dedicated spectral unmixing algorithm (Rakhymzhan et al. 2017) (for more details, see section *Image processing*).

The next element to consider is the fluorescence collection. Fluorescence photons are nearly always collected in non-descanned mode in intravital TPM, *i.e.*, without passing back through the scanning mirrors. They are instead reflected on a dichroic mirror situated between the objective and scanning mirrors, and are directed towards photomultiplier tubes (PMT), also known as non-descanned detectors (NDDs). In multicolor TPM, a number of NDDs is used. Fluorescence photons are discriminated according to their wavelengths using dichroic mirrors and filters. With such a setup, fluorescence arising from different fluorophores can be simultaneously collected on distinct detectors. Fluorescence intensity varies between the different used fluorophores according to parameters such as their quantity, their two-photon absorption cross-section (σ_2) and quantum yield (φ), the product of which defining the two-photon action cross-section ($\sigma_2\varphi$) listed in Tables 2-8. The emission wavelength of a fluorophore is another parameter influencing the collected intensity when put into perspective with the NDD response curve, high-energy blue photons being more absorbed than low-energy red photons in biological tissues (König 2000). When a single excitation is used, the laser intensity delivered to each of the fluorophores at the same observation depth will be identical. NDD gain should be adjusted accordingly for each of the fluorophores in order to enhance the signal over noise ratio, while avoiding saturating the detectors. When one expects a specific fluorescence signal to be low, more efficient PMTs such as Gallium Arsenide Phosphide (GaAsP) detectors should be considered (Becker et al. 2011).

Multicolor intravital TPM can benefit from the use of spectral chips, composed of an array of PMTs and a prism or diffraction grating to separate the fluorescence photons (Im et al. 2010; Shi et al. 2012, 2015; Zimmermann et al. 2014). Spectral segmentation of the

wavelengths arising for the different fluorophores will be thereby both more accurate and easier to achieve. Although such chips are already available on commercial confocal microscopes, they are positioned on the descanned path that is less suitable for intravital applications. Spectral chips in a non-descanned mode are required, and recent advances in non-descanned collection of fluorescence photons by optical fibers may help develop this approach (Ducros et al. 2011).

3.3 Image processing

Multicolor intravital timelapse TPM generates large amounts of data. The aim of the post-processing steps is to extract quantitative data and relevant characterization of the phenomenon of interest from multicolor acquisition.

When required, the first step is to perform spectral unmixing (Zimmermann et al. 2002; Neher and Neher 2004; Ducros et al. 2009). Even though the emission spectra of all of the fluorophores used in the experiment do not peak at the same wavelengths, there is generally a certain overlap of the spectra. As a consequence, the signal collected on one NDD contains a major contribution from one fluorophore and minor contributions from the others. It is possible to overcome this problem and to clean the image to retain only the contribution of the major fluorophore. To perform this spectral unmixing (*a.k.a.*, spectral deconvolution), the contribution of each of the fluorophores used in the experiment in each of the NDD must be measured. Then, using dedicated algorithms based on maximum-likelihood unmixing (Davis and Shen 2007), each image from each NDD can be spectrally unmixed and then analyzed (Thaler and Vogel 2006; Brenner et al. 2013; Zimmermann et al. 2014). As an example of the crucial importance of spectral unmixing, Ducros *et al.* have used it to detect small spectral variations of odor-evoked FRET transients up to 250 μm in the olfactory bulb of living mice (Ducros et al. 2009).

In another instance of multicolor intravital TPM experiment, Ricard *et al.* have recently proposed the 6-color intravital TPM of brain tumors (Ricard and Debarbieux 2014). They designed a triple transgenic Connexin43-**CFP**/Thy1-**GFP**/CD11c-**YFP** mouse model enabling the simultaneous observation of astrocytes, neurons, and microglia/dendritic cells, respectively. Mice were grafted under a chronic cranial window with glioblastoma cells expressing **DsRed**. Blood vessels were highlighted by an intravenous delivery of **Cascade Blue** dextran. Meninges were observed using SHG. Images were acquired on a microscope equipped with 5 NDDs under a sequential excitation at 800 and 940 nm. This sequential acquisition allows a discrimination of **CFP** and **Cascade Blue** signals as their two-photon excitation spectra are different, even though their emission spectra strongly overlap. After spectral unmixing, analysis revealed in particular significant alterations of cell motility in the peritumoral area.

The usefulness of spectral unmixing algorithms has become even clearer with the successful attempt to simultaneously detect up to 7 tissue compartments using two two-photon excitation sources and 6 NDDs (Rakhymzhan et al. 2017). In order to do this, the authors of this work developed a dedicated pixel-based algorithm based both on similarity measurements between overlapping fluorophores and on the spectral fingerprints of the individual fluorophores. As a result, the ‘SIMI’ algorithm enables the separation of more

fluorophores than available channels (*cf.* Figure 4). This protocol has been used in murine lymph nodes to simultaneously detect *in vivo* lymphocytes labelled with **Hoechst**, **CFP**, hrGFP, **YFP**, or **DsRed**, plus SHG and autofluorescence from macrophages.

Conclusion

Intravital TPM is a powerful tool to visualize biological phenomena with a subcellular resolution in a physiological environment. Multicolor TPM experiments make the most of the presence of all the actors – known or yet unknown – exhaustively involved in the complex processes that characterize brain functions. The design of intravital multicolor TPM experiments is, however, hindered at different stages following the identification of the biological targets of interest: choice of suitable fluorophores, choice of appropriate routes of delivery of these fluorophores, and design of the setup allowing simultaneous detection of various fluorophores.

This review was intended to reduce these hurdles by providing a comprehensive list of two-photon-suitable probes along with their spectral properties and biological specificities (*cf.* Tables 2 to 8), a description of different routes of *in vivo* delivery of these fluorophores (*cf.* Table 1), recommendations for the design of intravital multicolor TPM microscope setups, and a discussion about strategies of data post-processing. Taken together, this database and set of recommendations will help scientists design intravital TPM experiments focusing simultaneously on biological targets of diverse natures, ranging from cells (*e.g.*, neurons, astrocytes) and sub-cellular structures (*e.g.*, DNA, organelles) to functional processes – whose exploration greatly benefits from the optogenetics technology – (*e.g.*, ion transport, membrane potential), and through chemical or environmental parameters (*e.g.*, mechanical strains, pH) or even potentially connectomics (Nemoto et al. 2015).

Extending beyond the current trends in neuroscience, this comprehensive two-photon probe database, as well as the resources related to intravital multicolor TPM, is intended to broaden the use of TPM not only in neuroscience, but also to other fields of biology in which the full extent of this technology's capabilities has not yet been revealed.

Supplementary Material

Refer to Web version on PubMed Central for supplementary material.

Acknowledgments

Funding: CH is supported by a F30 Fellowship (NS093719 from NIH NINDS), as well as the UCLA Medical Scientist Training Program (NIH NIGMS training grant GM08042). CP-C is supported by W81XWH-14-1-0433 (USAMRMC, DOD), a Developmental Disabilities Translational Research Program grant (#20160969 from John Merck), SFARI Awards 295438 and 513155CP (Simons Foundation) and 5R01HD054453 (NICHD/NIH). GL is supported by the Agence Nationale de la Recherche (ANR-15-CE37-0004 "SmellBrain" & ANR-15-NEUC-0004 "Circuit_OPL").

Bibliography

Abdelfattah AS, Farhi SL, Zhao Y, et al. A Bright and Fast Red Fluorescent Protein Voltage Indicator That Reports Neuronal Activity in Organotypic Brain Slices. J Neurosci. 2016; 36:2458–72. DOI: 10.1523/JNEUROSCI.3484-15.2016 [PubMed: 26911693]

Acker CD, Yan P, Loew LM. Single-voxel recording of voltage transients in dendritic spines. Biophys J. 2011; 101:L11–3. DOI: 10.1016/j.bpj.2011.06.021 [PubMed: 21767473]

Ai H, Hazelwood KL, Davidson MW, Campbell RE. Fluorescent protein FRET pairs for ratiometric imaging of dual biosensors. Nat Methods. 2008; 5:401–3. DOI: 10.1038/nmeth.1207 [PubMed: 18425137]

Ai H, Henderson JN, Remington SJ, Campbell RE. Directed evolution of a monomeric, bright and photostable version of Clavularia cyan fluorescent protein: structural characterization and applications in fluorescence imaging. Biochem J. 2006; 400:531–40. DOI: 10.1042/BJ20060874 [PubMed: 16859491]

Akemann W, Sasaki M, Mutoh H, et al. Two-photon voltage imaging using a genetically encoded voltage indicator. Sci Rep. 2013; 3:2231.doi: 10.1038/srep02231 [PubMed: 23868559]

Akerboom J, Carreras Calderón N, Tian L, et al. Genetically encoded calcium indicators for multi-color neural activity imaging and combination with optogenetics. Front Mol Neurosci. 2013; 6:2.doi: 10.3389/fnmol.2013.00002 [PubMed: 23459413]

Akerboom J, Chen T-W, Wardill TJ, et al. Optimization of a GCaMP calcium indicator for neural activity imaging. J Neurosci. 2012; 32:13819–40. DOI: 10.1523/JNEUROSCI.2601-12.2012 [PubMed: 23035093]

Albota MA, Xu C, Webb WW. Two-Photon Fluorescence Excitation Cross Sections of Biomolecular Probes from 690 to 960 nm. Appl Opt. 1998; 37:7352–6. [PubMed: 18301569]

Anderson VL, Webb WW. Transmission electron microscopy characterization of fluorescently labelled amyloid β 1-40 and α-synuclein aggregates. BMC Biotechnol. 2011; 11:125.doi: 10.1186/1472-6750-11-125 [PubMed: 22182687]

Ando R, Flors C, Mizuno H, et al. Highlighted generation of fluorescence signals using simultaneous two-color irradiation on Dronpa mutants. Biophys J. 2007; 92:L97–9. DOI: 10.1529/biophysj.107.105882 [PubMed: 17384059]

Angevine JB, Sidman RL. Autoradiographic study of cell migration during histogenesis of cerebral cortex in the mouse. Nature. 1961; 192:766–768. DOI: 10.1038/192766b0

Appaix F, Girod S, Boisseau S, et al. Specific in vivo staining of astrocytes in the whole brain after intravenous injection of sulforhodamine dyes. PLoS One. 2012; 7:e35169.doi: 10.1371/journal.pone.0035169 [PubMed: 22509398]

Baek NY, Heo CH, Lim CS, et al. A highly sensitive two-photon fluorescent probe for mitochondrial zinc ions in living tissue. Chem Commun (Camb). 2012; 48:4546–8. DOI: 10.1039/c2cc31077e [PubMed: 22450755]

Baek Y, Park SJ, Zhou X, et al. A viscosity sensitive fluorescent dye for real-time monitoring of mitochondria transport in neurons. Biosens Bioelectron. 2016; 86:885–891. DOI: 10.1016/j.bios.2016.07.026 [PubMed: 27494813]

Bayerl SH, Niesner R, Cseresnyes Z, et al. Time lapse in vivo microscopy reveals distinct dynamics of microglia-tumor environment interactions-a new role for the tumor perivascular space as highway for trafficking microglia. Glia. 2016; 64:1210–26. DOI: 10.1002/glia.22994 [PubMed: 27143298]

Becker W, Su B, Holub O, Weisshart K. FLIM and FCS detection in laser-scanning microscopes: increased efficiency by GaAsP hybrid detectors. Microsc Res Tech. 2011; 74:804–11. DOI: 10.1002/jemt.20959 [PubMed: 23939667]

Bennewitz MF, Watkins SC, Sundd P. Quantitative intravital two-photon excitation microscopy reveals absence of pulmonary vaso-occlusion in unchallenged Sickle Cell Disease mice. IntraVital. 2014; 3:e29748.doi: 10.4161/intv.29748 [PubMed: 25995970]

Bestvater F, Spiess E, Stobrawa G, et al. Two-photon fluorescence absorption and emission spectra of dyes relevant for cell imaging. J Microsc. 2002; 208:108–115. DOI: 10.1046/j.1365-2818.2002.01074.x [PubMed: 12423261]

Blab GA, Lommerse PH, Cognet L, et al. Two-photon excitation action cross-sections of the autofluorescent proteins. Chem Phys Lett. 2001; 350:71–77. DOI: 10.1016/S0009-2614(01)01282-9

Bok S, Wang T, Lee C-J, et al. In vivo imaging of activated microglia in a mouse model of focal cerebral ischemia by two-photon microscopy. Biomed Opt Express. 2015; 6:3303–12. DOI: 10.1364/BOE.6.003303 [PubMed: 26417502]

Bonnin A, Torii M, Wang L, et al. Serotonin modulates the response of embryonic thalamocortical axons to netrin-1. Nat Neurosci. 2007; 10:588–597. DOI: 10.1038/nn1896 [PubMed: 17450135]

Borrell V, Yoshimura Y, Callaway EM. Targeted gene delivery to telencephalic inhibitory neurons by directional in utero electroporation. J Neurosci Methods. 2005; 143:151–158. DOI: 10.1016/j.jneumeth.2004.09.027 [PubMed: 15814147]

Brain KL, Bennett MR. Calcium in sympathetic varicosities of mouse vas deferens during facilitation, augmentation and autoinhibition. J Physiol. 1997; 502:521–536. DOI: 10.1111/j.1469-7793.1997.521bj.x [PubMed: 9279805]

Brenner MH, Cai D, Swanson JA, Ogilvie JP. Two-photon imaging of multiple fluorescent proteins by phase-shaping and linear unmixing with a single broadband laser. Opt Express. 2013; 21:17256–64. DOI: 10.1364/OE.21.017256 [PubMed: 23938572]

Brenowitz SD, Regehr WG. Presynaptic calcium measurements using bulk loading of acetoxymethyl indicators. Cold Spring Harb Protoc. 2014; 2014:750–7. DOI: 10.1101/pdb.prot081828 [PubMed: 24987144]

Brinks D, Klein AJ, Cohen AE. Two-Photon Lifetime Imaging of Voltage Indicating Proteins as a Probe of Absolute Membrane Voltage. Biophys J. 2015; 109:914–21. DOI: 10.1016/j.bpj.2015.07.038 [PubMed: 26331249]

Büning H, Huber A, Zhang L, et al. Engineering the AAV capsid to optimize vector-host-interactions. Curr Opin Pharmacol. 2015; 24:94–104. DOI: 10.1016/j.coph.2015.08.002 [PubMed: 26302254]

Burgold S, Bittner T, Dorostkar MM, et al. In vivo multiphoton imaging reveals gradual growth of newborn amyloid plaques over weeks. Acta Neuropathol. 2011; 121:327–35. DOI: 10.1007/s00401-010-0787-6 [PubMed: 21136067]

Cahalan MD, Parker I, Wei SH, Miller MJ. Two-photon tissue imaging: seeing the immune system in a fresh light. Nat Rev Immunol. 2002; 2:872–880. DOI: 10.1038/nri935 [PubMed: 12415310]

Caviness VS, Takahashi T. Proliferative events in the cerebral ventricular zone. Brain Dev. 1995; 17:159–163. DOI: 10.1016/0387-7604(95)00029-B [PubMed: 7573753]

Chaigneau E, Oheim M, Audinat E, Charpak S. Two-photon imaging of capillary blood flow in olfactory bulb glomeruli. Proc Natl Acad Sci U S A. 2003; 100:13081–6. DOI: 10.1073/pnas.2133652100 [PubMed: 14569029]

Chattopadhyay PK, Gaylord B, Palmer A, et al. Brilliant violet fluorophores: a new class of ultrabright fluorescent compounds for immunofluorescence experiments. Cytometry A. 2012; 81:456–66. DOI: 10.1002/cyto.a.22043 [PubMed: 22489009]

Chattoraj M, King BA, Bublitz GU, Boxer SG. Ultra-fast excited state dynamics in green fluorescent protein: multiple states and proton transfer. Proc Natl Acad Sci U S A. 1996; 93:8362–7. [PubMed: 8710876]

Chen Q, Cichon J, Wang W, et al. Imaging neural activity using Thy1-GCaMP transgenic mice. Neuron. 2012; 76:297–308. DOI: 10.1016/j.neuron.2012.07.011 [PubMed: 23083733]

Chen S, Zhao M, Su J, et al. Two novel two-photon excited fluorescent pH probes based on the A-π-D-π-A system for intracellular pH mapping. Dye Pigment. 2017; 136:807–816. DOI: 10.1016/j.dyepig.2016.09.020

Chen T-W, Wardill TJ, Sun Y, et al. Ultrasensitive fluorescent proteins for imaging neuronal activity. Nature. 2013; 499:295–300. DOI: 10.1038/nature12354 [PubMed: 23868258]

Chen Z, Kaplan DL, Yang K, et al. Two-photon-induced fluorescence from the phycoerythrin protein. Appl Opt. 1997; 36:1655–9. [PubMed: 18250850]

Chu J, Haynes RD, Corbel SY, et al. Non-invasive intravital imaging of cellular differentiation with a bright red-excitable fluorescent protein. Nat Methods. 2014; 11:572–8. DOI: 10.1038/nmeth.2888 [PubMed: 24633408]

Collot M, Loukou C, Yakovlev AV, et al. Calcium rubies: A family of red-emitting functionalizable indicators suitable for two-photon Ca2+ imaging. J Am Chem Soc. 2012; 134:14923–14931. DOI: 10.1021/ja304018d [PubMed: 22816677]

Crowe SE, Ellis-Davies GCR. Longitudinal in vivo two-photon fluorescence imaging. J Comp Neurol. 2014; 522:1708–27. DOI: 10.1002/cne.23502 [PubMed: 24214350]

Cruz-Martin A, Crespo M, Portera-Cailliau C. Delayed stabilization of dendritic spines in fragile X mice. J Neurosci. 2010; 30:7793–7803. [PubMed: 20534828]

Dana H, Chen T-W, Hu A, et al. Thy1-GCaMP6 Transgenic Mice for Neuronal Population Imaging In Vivo. PLoS One. 2014; 9:e108697.doi: 10.1371/journal.pone.0108697 [PubMed: 25250714]

Dana H, Mohar B, Sun Y, et al. Sensitive red protein calcium indicators for imaging neural activity. Elife. 2016; 5doi: 10.7554/eLife.12727

Danielyan A, Wu Y-W, Shih P-Y, et al. Denoising of two-photon fluorescence images with block-matching 3D filtering. Methods. 2014; 68:308–16. DOI: 10.1016/j.ymeth.2014.03.010 [PubMed: 24657185]

Danish IA, Lim CS, Tian YS, et al. Two-photon probes for Zn2+ ions with various dissociation constants. Detection of Zn2+ ions in live cells and tissues by two-photon microscopy. Chem Asian J. 2011; 6:1234–40. DOI: 10.1002/asia.201000720 [PubMed: 21337524]

Davis LM, Shen G. Extension of multidimensional microscopy to ultrasensitive applications with maximum-likelihood analysis. In: Conchello J-A, Cogswell CJ, Wilson T, editorsProc of SPIE. 2007. 64430N

Débarre D, Supatto W, Pena A-M, et al. Imaging lipid bodies in cells and tissues using third-harmonic generation microscopy. Nat Methods. 2006; 3:47–53. DOI: 10.1038/nmeth813 [PubMed: 16369553]

Deisseroth K. Optogenetics: 10 years of microbial opsins in neuroscience. Nat Neurosci. 2015; 18:1213–25. DOI: 10.1038/nn.4091 [PubMed: 26308982]

Denk W, Strickler JH, Webb WW. Two-photon laser scanning fluorescence microscopy. Science. 1990; 248:73–6. [PubMed: 2321027]

Dimitrov D, He Y, Mutoh H, et al. Engineering and characterization of an enhanced fluorescent protein voltage sensor. PLoS One. 2007; 2:e440.doi: 10.1371/journal.pone.0000440 [PubMed: 17487283]

Dong X, Han JH, Heo CH, et al. Dual-color imaging of magnesium/calcium ion activities with two-photon fluorescent probes. Anal Chem. 2012; 84:8110–3. DOI: 10.1021/ac302210v [PubMed: 22967146]

Dray N, Bedu S, Vuillemin N, et al. Large-scale live imaging of adult neural stem cells in their endogenous niche. Development. 2015; 142:3592–600. DOI: 10.1242/dev.123018 [PubMed: 26395477]

Drobizhev M, Makarov NS, Tillo SE, et al. Two-photon absorption properties of fluorescent proteins. Nat Methods. 2011; 8:393–9. DOI: 10.1038/nmeth.1596 [PubMed: 21527931]

Drobizhev M, Tillo S, Makarov NS, et al. Absolute two-photon absorption spectra and two-photon brightness of orange and red fluorescent proteins. J Phys Chem B. 2009; 113:855–9. DOI: 10.1021/jp8087379 [PubMed: 19127988]

Ducros M, Moreaux L, Bradley J, et al. Spectral unmixing: analysis of performance in the olfactory bulb in vivo. PLoS One. 2009; 4:e4418.doi: 10.1371/journal.pone.0004418 [PubMed: 19198655]

Ducros M, van 't Hoff M, van't Hoff M, et al. Efficient large core fiber-based detection for multi-channel two-photon fluorescence microscopy and spectral unmixing. J Neurosci Methods. 2011; 198:172–80. DOI: 10.1016/j.jneumeth.2011.03.015 [PubMed: 21458489]

Emiliani V, Cohen AE, Deisseroth K, Häusser M. All-Optical Interrogation of Neural Circuits. J Neurosci. 2015; 35:13917–26. DOI: 10.1523/JNEUROSCI.2916-15.2015 [PubMed: 26468193]

Eriksson A, Österroos A, Hassan S, et al. Drug screen in patient cells suggests quinacrine to be repositioned for treatment of acute myeloid leukemia. Blood Cancer J. 2015; 5:e307.doi: 10.1038/bcj.2015.31 [PubMed: 25885427]

Estrada G, Beetle C, Schummers J. Simple method to improve spatial resolution for in vivo two-photon fluorescence imaging. Appl Opt. 2015; 54:10044–50. [PubMed: 26836658]

Feng G, Mellor RH, Bernstein M, et al. Imaging neuronal subsets in transgenic mice expressing multiple spectral variants of GFP. Neuron. 2000; 28:41–51. [PubMed: 11086982]

Fenrich KK, Weber P, Hocine M, et al. Long-term in vivo imaging of normal and pathological mouse spinal cord with subcellular resolution using implanted glass windows. J Physiol. 2012; 590:3665–75. DOI: 10.1113/jphysiol.2012.230532 [PubMed: 22641787]

Fenrich KK, Weber P, Rougon G, Debarbieux F. Long- and short-term intravital imaging reveals differential spatiotemporal recruitment and function of myelomonocytic cells after spinal cord injury. J Physiol. 2013; 591:4895–902. DOI: 10.1113/jphysiol.2013.256388 [PubMed: 23918770]

Ferezou I, Bolea S, Petersen CCH. Visualizing the cortical representation of whisker touch: voltage-sensitive dye imaging in freely moving mice. Neuron. 2006; 50:617–29. DOI: 10.1016/j.neuron.2006.03.043 [PubMed: 16701211]

Filonov GS, Piatkevich KD, Ting L-M, et al. Bright and stable near-infrared fluorescent protein for in vivo imaging. Nat Biotechnol. 2011; 29:757–61. DOI: 10.1038/nbt.1918 [PubMed: 21765402]

Fiole D, Deman P, Trescos Y, et al. Two-photon intravital imaging of lungs during anthrax infection reveals long-lasting macrophage-dendritic cell contacts. Infect Immun. 2014; 82:864–72. DOI: 10.1128/IAI.01184-13 [PubMed: 24478099]

Fisher JAN, Barchi JR, Welle CG, et al. Two-photon excitation of potentiometric probes enables optical recording of action potentials from mammalian nerve terminals in situ. J Neurophysiol. 2008; 99:1545–53. DOI: 10.1152/jn.00929.2007 [PubMed: 18171710]

Fisher JAN, Salzberg BM, Yodh AG. Near infrared two-photon excitation cross-sections of voltage-sensitive dyes. J Neurosci Methods. 2005; 148:94–102. DOI: 10.1016/j.jneumeth.2005.06.027 [PubMed: 16129493]

Frantsuzov PA, Volkán-Kacsó S, Jankó B. Universality of the fluorescence intermittency in nanoscale systems: experiment and theory. Nano Lett. 2013; 13:402–8. DOI: 10.1021/nl3035674 [PubMed: 23272638]

Frey W, White JA, Price RO, et al. Plasma membrane voltage changes during nanosecond pulsed electric field exposure. Biophys J. 2006; 90:3608–15. DOI: 10.1529/biophysj.105.072777 [PubMed: 16513782]

Fujii S, Hirota A, Kamino K. Action potential synchrony in embryonic precontractile chick heart: optical monitoring with potentiometric dyes. J Physiol. 1981; 319:529–41. [PubMed: 7320925]

Fukuchi-Shimogori T, Grove EA. Neocortex Patterning by the Secreted Signaling Molecule FGF8. Science (80-). 2001; 294

Galli R, Uckermann O, Andresen EF, et al. Intrinsic indicator of photodamage during label-free multiphoton microscopy of cells and tissues. PLoS One. 2014; 9:e110295.doi: 10.1371/journal.pone.0110295 [PubMed: 25343251]

Garaschuk O, Milos R-I, Konnerth A. Targeted bulk-loading of fluorescent indicators for two-photon brain imaging in vivo. Nat Protoc. 2006; 1:380–6. DOI: 10.1038/nprot.2006.58 [PubMed: 17406260]

Gee KR, Brown KA, Chen WN, et al. Chemical and physiological characterization of fluo-4 Ca(2+)-indicator dyes. Cell Calcium. 2000; 27:97–106. DOI: 10.1054/ceca.1999.0095 [PubMed: 10756976]

Grienberger C, Chen X, Konnerth A. NMDA Receptor-Dependent Multidendrite Ca(2+) Spikes Required for Hippocampal Burst Firing In Vivo. Neuron. 2014; 81:1274–1281. DOI: 10.1016/j.neuron.2014.01.014 [PubMed: 24560703]

Grienberger C, Konnerth A. Imaging calcium in neurons. Neuron. 2012; 73:862–85. DOI: 10.1016/j.neuron.2012.02.011 [PubMed: 22405199]

Griesbeck O, Baird GS, Campbell RE, et al. Reducing the environmental sensitivity of yellow fluorescent protein. Mechanism and applications. J Biol Chem. 2001; 276:29188–94. DOI: 10.1074/jbc.M102815200 [PubMed: 11387331]

Grinvald A, Hildesheim R. VSDI: a new era in functional imaging of cortical dynamics. Nat Rev Neurosci. 2004; 5:874–85. DOI: 10.1038/nrn1536 [PubMed: 15496865]

Grynkiewicz G, Poenie M, Tsien RY. A new generation of Ca2+ indicators with greatly improved fluorescence properties. J Biol Chem. 1985; 260:3440–3450. doi: 3838314. [PubMed: 3838314]

Han JH, Park SK, Lim CS, et al. Simultaneous imaging of mitochondria and lysosomes by using two-photon fluorescent probes. Chemistry. 2012; 18:15246–9. DOI: 10.1002/chem.201203452 [PubMed: 23112112]

Hashimoto H, Isobe K, Suda A, et al. Measurement of two-photon excitation spectra of fluorescent proteins with nonlinear Fourier-transform spectroscopy. Appl Opt. 2010; 49:3323–9. [PubMed: 20539351]

Heinze KG, Koltermann A, Schwille P. Simultaneous two-photon excitation of distinct labels for dual-color fluorescence crosscorrelation analysis. Proc Natl Acad Sci U S A. 2000; 97:10377–82. DOI: 10.1073/pnas.180317197 [PubMed: 10973482]

Helassa N, Zhang X, Conte I, et al. Fast-Response Calmodulin-Based Fluorescent Indicators Reveal Rapid Intracellular Calcium Dynamics. Sci Rep. 2015; 5:15978.doi: 10.1038/srep15978 [PubMed: 26527405]

Helmchen F. Two-Photon Functional Imaging of Neuronal Activity. 2009

Helmchen F, Denk W. Deep tissue two-photon microscopy. Nat Methods. 2005; 2:932–40. DOI: 10.1038/nmeth818 [PubMed: 16299478]

Heo CH, Kim KH, Kim HJ, et al. A two-photon fluorescent probe for amyloid-β plaques in living mice. Chem Commun (Camb). 2013; 49:1303–5. DOI: 10.1039/c2cc38570h [PubMed: 23295364]

Herron TJ, Lee P, Jalife J. Optical imaging of voltage and calcium in cardiac cells & tissues. Circ Res. 2012; 110:609–623. DOI: 10.1161/CIRCRESAHA.111.247494 [PubMed: 22343556]

Herz J, Siffrin V, Hauser AE, et al. Expanding two-photon intravital microscopy to the infrared by means of optical parametric oscillator. Biophys J. 2010; 98:715–23. DOI: 10.1016/j.bpj.2009.10.035 [PubMed: 20159168]

Hess GP, Lewis RW, Chen Y. Caged neurotransmitters and other caged compounds: design and application. Cold Spring Harb Protoc. 2014; 2014 pdb.top084152. doi: 10.1101/pdb.top084152

Holtmaat A, Bonhoeffer T, Chow DK, et al. Long-term, high-resolution imaging in the mouse neocortex through a chronic cranial window. Nat Protoc. 2009; 4:1128–44. DOI: 10.1038/nprot.2009.89 [PubMed: 19617885]

Huber D, Petreanu L, Ghitani N, et al. Sparse optical microstimulation in barrel cortex drives learned behaviour in freely moving mice. Nature. 2008; 451:61–64. doi: nature06445 [pii] 10.1038/nature06445. [PubMed: 18094685]

Im K-B, Kang M-S, Kim J, et al. Two-photon spectral imaging with high temporal and spectral resolution. Opt Express. 2010; 18:26905–14. DOI: 10.1364/OE.18.026905 [PubMed: 21196967]

Ji N, Milkie DE, Betzig E. Adaptive optics via pupil segmentation for high-resolution imaging in biological tissues. Nat Methods. 2010; 7:141–7. DOI: 10.1038/nmeth.1411 [PubMed: 20037592]

Jin L, Han Z, Platisa J, et al. Single action potentials and subthreshold electrical events imaged in neurons with a fluorescent protein voltage probe. Neuron. 2012; 75:779–85. DOI: 10.1016/j.neuron.2012.06.040 [PubMed: 22958819]

Jung S, Aliberti J, Graemmel P, et al. Analysis of fractalkine receptor CX(3)CR1 function by targeted deletion and green fluorescent protein reporter gene insertion. Mol Cell Biol. 2000; 20:4106–14. [PubMed: 10805752]

Junyent F, Kremer EJ. CAV-2–why a canine virus is a neurobiologist's best friend. Curr Opin Pharmacol. 2015; 24:86–93. DOI: 10.1016/j.coph.2015.08.004 [PubMed: 26298516]

Kamino K, Katoh Y, Komuro H, Sato K. Multiple-site optical monitoring of neural activity evoked by vagus nerve stimulation in the embryonic chick brain stem. J Physiol. 1989; 409:263–83. [PubMed: 2585291]

Kandel ER, Schwartz JH, Jessell TM. Principles of Neural Science. 4th. McGraw-Hill; 2000.

Kao Y-T, Zhu X, Xu F, Min W. Focal switching of photochromic fluorescent proteins enables multiphoton microscopy with superior image contrast. Biomed Opt Express. 2012; 3:1955–63. DOI: 10.1364/BOE.3.001955 [PubMed: 22876358]

Karasawa S, Araki T, Nagai T, et al. Cyan-emitting and orange-emitting fluorescent proteins as a donor/acceptor pair for fluorescence resonance energy transfer. Biochem J. 2004; 381:307–12. DOI: 10.1042/BJ20040321 [PubMed: 15065984]

Keikhosravi A, Bredfeldt JS, Sagar AK, Eliceiri KW. Second-harmonic generation imaging of cancer. Methods Cell Biol. 2014; 123:531–46. DOI: 10.1016/B978-0-12-420138-5.00028-8 [PubMed: 24974046]

Khan M, Goldsmith CR, Huang Z, et al. Two-photon imaging of Zn2+ dynamics in mossy fiber boutons of adult hippocampal slices. Proc Natl Acad Sci U S A. 2014; 111:6786–91. DOI: 10.1073/pnas.1405154111 [PubMed: 24757053]

Kim HJ, Han JH, Kim MK, et al. Dual-color imaging of sodium/calcium ion activities with two-photon fluorescent probes. Angew Chem Int Ed Engl. 2010a; 49:6786–9. DOI: 10.1002/anie.201002907 [PubMed: 20715036]

Kim HM, Choo H-J, Jung S-Y, et al. A two-photon fluorescent probe for lipid raft imaging: C-laurdan. Chembiochem. 2007; 8:553–9. DOI: 10.1002/cbic.200700003 [PubMed: 17300111]

Kim HM, Kim BR, An MJ, et al. Two-photon fluorescent probes for long-term imaging of calcium waves in live tissue. Chemistry. 2008a; 14:2075–83. DOI: 10.1002/chem.200701453 [PubMed: 18175306]

Kim HM, Seo MS, An MJ, et al. Two-photon fluorescent probes for intracellular free zinc ions in living tissue. Angew Chem Int Ed Engl. 2008b; 47:5167–70. DOI: 10.1002/anie.200800929 [PubMed: 18528837]

Kim JH, Lee S-R, Li L-H, et al. High Cleavage Efficiency of a 2A Peptide Derived from Porcine Teschovirus-1 in Human Cell Lines, Zebrafish and Mice. PLoS One. 2011; 6:e18556.doi: 10.1371/journal.pone.0018556 [PubMed: 21602908]

Kim MK, Lim CS, Hong JT, et al. Sodium-ion-selective two-photon fluorescent probe for in vivo imaging. Angew Chem Int Ed Engl. 2010b; 49:364–7. DOI: 10.1002/anie.200904835 [PubMed: 19998298]

Klunk WE, Bacskai BJ, Mathis CA, et al. Imaging Abeta plaques in living transgenic mice with multiphoton microscopy and methoxy-X04, a systemically administered Congo red derivative. J Neuropathol Exp Neurol. 2002; 61:797–805. [PubMed: 12230326]

Kobat D, Durst ME, Nishimura N, et al. Deep tissue multiphoton microscopy using longer wavelength excitation. Opt Express. 2009; 17:13354–13364. DOI: 10.1364/OE.17.013354 [PubMed: 19654740]

Kobat D, Horton NG, Xu C. In vivo two-photon microscopy to 1.6-mm depth in mouse cortex. J Biomed Opt. 2011; 16:106014.doi: 10.1117/1.3646209 [PubMed: 22029361]

König K. Multiphoton microscopy in life sciences. J Microsc. 2000; 200:83–104. [PubMed: 11106949]

Kristianto J, Johnson MG, Zastrow RK, et al. Spontaneous recombinase activity of Cre-ERT2 in vivo. Transgenic Res. 2017; 26:411–417. DOI: 10.1007/s11248-017-0018-1 [PubMed: 28409408]

Kuhn B, Denk W, Bruno RM. In vivo two-photon voltage-sensitive dye imaging reveals top-down control of cortical layers 1 and 2 during wakefulness. Proc Natl Acad Sci U S A. 2008; 105:7588–93. DOI: 10.1073/pnas.0802462105 [PubMed: 18508976]

Kuhn B, Fromherz P, Denk W. High sensitivity of Stark-shift voltage-sensing dyes by one- or two-photon excitation near the red spectral edge. Biophys J. 2004; 87:631–9. DOI: 10.1529/biophysj.104.040477 [PubMed: 15240496]

Kuwashima N, Nishimura F, Eguchi J, et al. Delivery of dendritic cells engineered to secrete IFN-alpha into central nervous system tumors enhances the efficacy of peripheral tumor cell vaccines: dependence on apoptotic pathways. J Immunol. 2005; 175:2730–40. [PubMed: 16081851]

Lane LA, Smith AM, Lian T, Nie S. Compact and blinking-suppressed quantum dots for single-particle tracking in live cells. J Phys Chem B. 2014; 118:14140–7. DOI: 10.1021/jp5064325 [PubMed: 25157589]

Langer J, Rose CR. Synaptically induced sodium signals in hippocampal astrocytes in situ. J Physiol. 2009; 587:5859–77. DOI: 10.1113/jphysiol.2009.182279 [PubMed: 19858225]

Larson DR, Zipfel WR, Williams RM, et al. Water-soluble quantum dots for multiphoton fluorescence imaging in vivo. Science. 2003; 300:1434–6. DOI: 10.1126/science.1083780 [PubMed: 12775841]

Lee JH, Lim CS, Tian YS, et al. A two-photon fluorescent probe for thiols in live cells and tissues. J Am Chem Soc. 2010; 132:1216–7. DOI: 10.1021/ja9090676 [PubMed: 20052975]

Lee S, Lee JH, Park JH, et al. In vivo 3D measurement of moxifloxacin and gatifloxacin distributions in the mouse cornea using multiphoton microscopy. Sci Rep. 2016; 6:25339.doi: 10.1038/srep25339 [PubMed: 27138688]

Li W, Fang B, Jin M, Tian Y. Two-Photon Ratiometric Fluorescence Probe with Enhanced Absorption Cross Section for Imaging and Biosensing of Zinc Ions in Hippocampal Tissue and Zebrafish. Anal Chem. 2017; 89:2553–2560. DOI: 10.1021/acs.analchem.6b04781 [PubMed: 28192925]

Lim CS, Cho BR. Two-photon probes for biomedical applications. BMB Rep. 2013; 46:188–94. DOI: 10.5483/BMBRep.2013.46.4.045 [PubMed: 23615259]

Lim CS, Chung C, Kim HM, et al. A two-photon turn-on probe for glucose uptake. Chem Commun (Camb). 2012; 48:2122–4. DOI: 10.1039/c2cc16792a [PubMed: 22249940]

Lim CS, Kang MY, Han JH, et al. In vivo imaging of near-membrane calcium ions with two-photon probes. Chem Asian J. 2011a; 6:2028–33. DOI: 10.1002/asia.201100156 [PubMed: 21688396]

Lim CS, Kim HJ, Lee JH, et al. A two-photon turn-on probe for lipid rafts with minimum internalization. Chembiochem. 2011b; 12:392–5. DOI: 10.1002/cbic.201000609 [PubMed: 21290540]

Lippes J. Quinacrine sterilization (QS): time for reconsideration. Contraception. 2015; 92:91–5. DOI: 10.1016/j.contraception.2015.06.005 [PubMed: 26072742]

Liu H-W, Xu S, Wang P, et al. An efficient two-photon fluorescent probe for monitoring mitochondrial singlet oxygen in tissues during photodynamic therapy. Chem Commun (Camb). 2016; 52:12330–12333. DOI: 10.1039/c6cc05880a [PubMed: 27722455]

Liu XF, Haas K. Single-cell electroporation of Xenopus tadpole tectal neurons. Cold Spring Harb Protoc. 2011; 2011doi: 10.1101/pdb.prot065615

Livet J, Weissman TA, Kang H, et al. Transgenic strategies for combinatorial expression of fluorescent proteins in the nervous system. Nature. 2007; 450:56–62. DOI: 10.1038/nature06293 [PubMed: 17972876]

Loew LM, Lewis A. Second Harmonic Imaging of Membrane Potential. Adv Exp Med Biol. 2015; 859:473–92. DOI: 10.1007/978-3-319-17641-3_19 [PubMed: 26238065]

Looger LL, Griesbeck O. Genetically encoded neural activity indicators. Curr Opin Neurobiol. 2011; 22:18–23. DOI: 10.1016/j.conb.2011.10.024 [PubMed: 22104761]

Lukomska J, Gryczynski I, Malicka J, et al. One- and two-photon induced fluorescence of Pacific Blue-labeled human serum albumin deposited on different core size silver colloids. Biopolymers. 2006; 81:249–55. DOI: 10.1002/bip.20407 [PubMed: 16273526]

Lundby A, Mutoh H, Dimitrov D, et al. Engineering of a genetically encodable fluorescent voltage sensor exploiting fast Ci-VSP voltage-sensing movements. PLoS One. 2008; 3:e2514.doi: 10.1371/journal.pone.0002514 [PubMed: 18575613]

Mahou P, Zimmerley M, Loulier K, et al. Multicolor two-photon tissue imaging by wavelength mixing. Nat Methods. 2012; 9:815–8. DOI: 10.1038/nmeth.2098 [PubMed: 22772730]

Manent J-B, Wang Y, Chang Y, et al. Dcx reexpression reduces subcortical band heterotopia and seizure threshold in an animal model of neuronal migration disorder. Nat Med. 2009; 15:84–90. DOI: 10.1038/nm.1897 [PubMed: 19098909]

Mank M, Santos AF, Direnberger S, et al. A genetically encoded calcium indicator for chronic in vivo two-photon imaging. Nat Methods. 2008; 5:805–811. DOI: 10.1038/nmeth.1243 [PubMed: 19160515]

Marchuk K, Guo Y, Sun W, et al. High-precision tracking with non-blinking quantum dots resolves nanoscale vertical displacement. J Am Chem Soc. 2012; 134:6108–11. DOI: 10.1021/ja301332t [PubMed: 22458433]

Marshall JD, Li JZ, Zhang Y, et al. Cell-Type-Specific Optical Recording of Membrane Voltage Dynamics in Freely Moving Mice. Cell. 2016; 167:1650–1662.e15. DOI: 10.1016/j.cell.2016.11.021 [PubMed: 27912066]

Marvin JS, Borghuis BG, Tian L, et al. An optimized fluorescent probe for visualizing glutamate neurotransmission. Nat Methods. 2013; 10:162–70. DOI: 10.1038/nmeth.2333 [PubMed: 23314171]

Masanta G, Lim CS, Kim HJ, et al. A mitochondrial-targeted two-photon probe for zinc ion. J Am Chem Soc. 2011; 133:5698–700. DOI: 10.1021/ja200444t [PubMed: 21449534]

Mashinchian O, Johari-Ahar M, Ghaemi B, et al. Impacts of quantum dots in molecular detection and bioimaging of cancer. Bioimpacts. 2014; 4:149–66. DOI: 10.15171/bi.2014.008 [PubMed: 25337468]

Matsuda T, Cepko CL. Electroporation and RNA interference in the rodent retina in vivo and in vitro. Proc Natl Acad Sci U S A. 2004; 101:16–22. [PubMed: 14603031]

Matsuda T, Cepko CL. Controlled expression of transgenes introduced by in vivo electroporation. Proc Natl Acad Sci U S A. 2007; 104:1027–32. DOI: 10.1073/pnas.0610155104 [PubMed: 17209010]

Merzlyak EM, Goedhart J, Shcherbo D, et al. Bright monomeric red fluorescent protein with an extended fluorescence lifetime. Nat Methods. 2007; 4:555–7. DOI: 10.1038/nmeth1062 [PubMed: 17572680]

Mettra B, Appaix F, Olesiak-Banska J, et al. A Fluorescent Polymer Probe with High Selectivity toward Vascular Endothelial Cells for and beyond Noninvasive Two-Photon Intravital Imaging of Brain Vasculature. ACS Appl Mater Interfaces. 2016; 8:17047–59. DOI: 10.1021/acsami.6b02936 [PubMed: 27267494]

Miao F, Zhang W, Sun Y, et al. Novel fluorescent probes for highly selective two-photon imaging of mitochondria in living cells. Biosens Bioelectron. 2014; 55:423–9. DOI: 10.1016/j.bios.2013.12.044 [PubMed: 24441022]

Miller MJ, Wei SH, Parker I, Cahalan MD. Two-photon imaging of lymphocyte motility and antigen response in intact lymph node. Science. 2002; 296:1869–73. DOI: 10.1126/science.1070051 [PubMed: 12016203]

Miyawaki A, Llopis J, Heim R, et al. Fluorescent indicators for Ca2+ based on green fluorescent proteins and calmodulin. Nature. 1997; 388:882–887. DOI: 10.1038/42264 [PubMed: 9278050]

Miyazaki K, Ross WN. Simultaneous Sodium and Calcium Imaging from Dendrites and Axons. eNeuro. 2015; 2:1–10. DOI: 10.1523/ENEURO.0092-15.2015

Mohan PS, Lim CS, Tian YS, et al. A two-photon fluorescent probe for near-membrane calcium ions in live cells and tissues. Chem Commun (Camb). 2009; :5365–7. DOI: 10.1039/b911337a [PubMed: 19724786]

Mojzisova H, Vermot J. When multiphoton microscopy sees near infrared. Curr Opin Genet Dev. 2011; 21:549–57. DOI: 10.1016/j.gde.2011.08.004 [PubMed: 21924603]

Momose-Sato Y, Sato K, Kamino K. Optical approaches to embryonic development of neural functions in the brainstem. Prog Neurobiol. 2001; 63:151–97. [PubMed: 11124445]

Morelli AE, Larregina AT, Shufesky WJ, et al. Internalization of circulating apoptotic cells by splenic marginal zone dendritic cells: dependence on complement receptors and effect on cytokine production. Blood. 2003; 101:611–20. DOI: 10.1182/blood-2002-06-1769 [PubMed: 12393562]

Moritomo H, Yamada K, Kojima Y, et al. A biphenyl type two-photon fluorescence probe for monitoring the mitochondrial membrane potential. Cell Struct Funct. 2014; 39:125–33. DOI: 10.1247/csf.14006 [PubMed: 25319070]

Mossakowski AA, Pohlan J, Bremer D, et al. Tracking CNS and systemic sources of oxidative stress during the course of chronic neuroinflammation. Acta Neuropathol. 2015; 130:799–814. DOI: 10.1007/s00401-015-1497-x [PubMed: 26521072]

Mostany R, Miquelajauregui A, Shtrahman M, Portera-Cailliau C. Two-photon excitation microscopy and its applications in neuroscience. Methods Mol Biol. 2015; 1251:25–42. DOI: 10.1007/978-1-4939-2080-8_2 [PubMed: 25391792]

Murphy TH, Li P, Betts K, Liu R. Two-photon imaging of stroke onset in vivo reveals that NMDA-receptor independent ischemic depolarization is the major cause of rapid reversible damage to dendrites and spines. J Neurosci. 2008; 28:1756–72. DOI: 10.1523/JNEUROSCI.5128-07.2008 [PubMed: 18272696]

Mütze J, Iyer V, Macklin JJ, et al. Excitation spectra and brightness optimization of two-photon excited probes. Biophys J. 2012; 102:934–44. DOI: 10.1016/j.bpj.2011.12.056 [PubMed: 22385865]

Myoga MH, Beierlein M, Regehr WG. Somatic spikes regulate dendritic signaling in small neurons in the absence of backpropagating action potentials. J Neurosci. 2009; 29:7803–14. DOI: 10.1523/JNEUROSCI.0030-09.2009 [PubMed: 19535592]

Nagai T, Ibata K, Park ES, et al. A variant of yellow fluorescent protein with fast and efficient maturation for cell-biological applications. Nat Biotechnol. 2002; 20:87–90. DOI: 10.1038/nbt0102-87 [PubMed: 11753368]

Nagai T, Yamada S, Tominaga T, et al. Expanded dynamic range of fluorescent indicators for Ca(2+) by circularly permuted yellow fluorescent proteins. Proc Natl Acad Sci U S A. 2004; 101:10554–10559. DOI: 10.1073/pnas.0400417101 [PubMed: 15247428]

Nakahira E, Kagawa T, Shimizu T, et al. Direct evidence that ventral forebrain cells migrate to the cortex and contribute to the generation of cortical myelinating oligodendrocytes. Dev Biol. 2006; 291:123–131. DOI: 10.1016/j.ydbio.2005.12.010 [PubMed: 16413527]

Nakai J, Ohkura M, Imoto K. A high signal-to-noise Ca(2+) probe composed of a single green fluorescent protein. Nat Biotechnol. 2001; 19:137–41. DOI: 10.1038/84397 [PubMed: 11175727]

Nassi JJ, Cepko CL, Born RT, Beier KT. Neuroanatomy goes viral! Front Neuroanat. 2015; 9:80.doi: 10.3389/fnana.2015.00080 [PubMed: 26190977]

Navarro-Quiroga I, Chittajallu R, Gallo V, Haydar TF. Long-Term, Selective Gene Expression in Developing and Adult Hippocampal Pyramidal Neurons Using Focal In Utero Electroporation. J Neurosci. 2007; 27

Neher R, Neher E. Optimizing imaging parameters for the separation of multiple labels in a fluorescence image. J Microsc. 2004; 213:46–62. [PubMed: 14678512]

Nemoto T, Kawakami R, Hibi T, et al. Two-photon excitation fluorescence microscopy and its application in functional connectomics. Reprod Syst Sex Disord. 2015; 64:9–15. DOI: 10.1093/jmicro/dfu110

Neu TR, Kuhlicke U, Lawrence JR. Assessment of fluorochromes for two-photon laser scanning microscopy of biofilms. Appl Environ Microbiol. 2002; 68:901–9. [PubMed: 11823234]

Nimmerjahn A, Kirchhoff F, Kerr JND, Helmchen F. Sulforhodamine 101 as a specific marker of astroglia in the neocortex in vivo. Nat Methods. 2004; 1:31–7. DOI: 10.1038/nmeth706 [PubMed: 15782150]

Packer AM, Russell LE, Dalgleish HWP, Häusser M. Simultaneous all-optical manipulation and recording of neural circuit activity with cellular resolution in vivo. Nat Methods. 2015; 12:140–6. DOI: 10.1038/nmeth.3217 [PubMed: 25532138]

Pak YL, Swamy KMK, Yoon J. Recent Progress in Fluorescent Imaging Probes. Sensors (Basel). 2015; 15:24374–96. DOI: 10.3390/s150924374 [PubMed: 26402684]

Papagiakoumou E, Bègue A, Leshem B, et al. Functional patterned multiphoton excitation deep inside scattering tissue. Nat Photonics. 2013; 7:274–278. DOI: 10.1038/nphoton.2013.9

Park HJ, Lim CS, Kim ES, et al. Measurement of pH values in human tissues by two-photon microscopy. Angew Chem Int Ed Engl. 2012; 51:2673–6. DOI: 10.1002/anie.201109052 [PubMed: 22298491]

Petersen CCH, Grinvald A, Sakmann B. Spatiotemporal dynamics of sensory responses in layer 2/3 of rat barrel cortex measured in vivo by voltage-sensitive dye imaging combined with whole-cell voltage recordings and neuron reconstructions. J Neurosci. 2003; 23:1298–309. [PubMed: 12598618]

Petrat F, Rauen U, de Groot H. Determination of the chelatable iron pool of isolated rat hepatocytes by digital fluorescence microscopy using the fluorescent probe, phen green SK. Hepatology. 1999; 29:1171–9. DOI: 10.1002/hep.510290435 [PubMed: 10094962]

Piatkevich KD, Hulit J, Subach OM, et al. Monomeric red fluorescent proteins with a large Stokes shift. Proc Natl Acad Sci U S A. 2010; 107:5369–74. DOI: 10.1073/pnas.0914365107 [PubMed: 20212155]

Podgorski K, Terpetschnig E, Klochko OP, et al. Ultra-bright and -stable red and near-infrared squaraine fluorophores for in vivo two-photon imaging. PLoS One. 2012; 7:e51980.doi: 10.1371/journal.pone.0051980 [PubMed: 23251670]

Pond SJK, Rumi M, Levin MD, et al. One- and Two-Photon Spectroscopy of Donor-Acceptor-Donor Distyrylbenzene Derivatives: Effect of Cyano Substitution and Distortion from Planarity. J Phys Chem A. 2002; 106:11470–11480. DOI: 10.1021/jp0267104

Porrero C, Rubio-Garrido P, Avendaño C, Clascá F. Mapping of fluorescent protein-expressing neurons and axon pathways in adult and developing Thy1-eYFP-H transgenic mice. Brain Res. 2010; 1345:59–72. DOI: 10.1016/j.brainres.2010.05.061 [PubMed: 20510892]

Poulet JFA, Petersen CCH. Internal brain state regulates membrane potential synchrony in barrel cortex of behaving mice. Nature. 2008; 454:881–5. DOI: 10.1038/nature07150 [PubMed: 18633351]

Powell SK, Khan N, Parker CL, et al. Characterization of a novel adeno-associated viral vector with preferential oligodendrocyte tropism. Gene Ther. 2016; 23:807–814. DOI: 10.1038/gt.2016.62 [PubMed: 27628693]

Prakash R, Yizhar O, Grewe B, et al. Two-photon optogenetic toolbox for fast inhibition, excitation and bistable modulation. Nat Methods. 2012; 9:1171–9. DOI: 10.1038/nmeth.2215 [PubMed: 23169303]

Radbruch H, Bremer D, Guenther R, et al. Ongoing Oxidative Stress Causes Subclinical Neuronal Dysfunction in the Recovery Phase of EAE. Front Immunol. 2016; 7:92.doi: 10.3389/fimmu.2016.00092 [PubMed: 27014271]

Rakhymzhan A, Leben R, Zimmermann H, et al. Synergistic Strategy for Multicolor Two-photon Microscopy: Application to the Analysis of Germinal Center Reactions In Vivo. Sci Rep. 2017; 7:7101.doi: 10.1038/s41598-017-07165-0 [PubMed: 28769068]

Rakic P. Neurons in Rhesus Monkey Visual Cortex: Systematic Relation between Time of Origin and Eventual Disposition. Science (80-). 1974; 183

Rama S, Vetrivel L, Semyanov A. Second-harmonic generation voltage imaging at subcellular resolution in rat hippocampal slices. J Biophotonics. 2010; 3:784–90. DOI: 10.1002/jbio.201000073 [PubMed: 20815024]

Reeves AMB, Shigetomi E, Khakh BS. Bulk loading of calcium indicator dyes to study astrocyte physiology: key limitations and improvements using morphological maps. J Neurosci. 2011; 31:9353–8. DOI: 10.1523/JNEUROSCI.0127-11.2011 [PubMed: 21697385]

Resendez SL, Jennings JH, Ung RL, et al. Visualization of cortical, subcortical and deep brain neural circuit dynamics during naturalistic mammalian behavior with head-mounted microscopes and chronically implanted lenses. Nat Protoc. 2016; 11:566–97. DOI: 10.1038/nprot.2016.021 [PubMed: 26914316]

Ricard C, Debarbieux FC. Six-color intravital two-photon imaging of brain tumors and their dynamic microenvironment. Front Cell Neurosci. 2014; 8:57.doi: 10.3389/fncel.2014.00057 [PubMed: 24605087]

Ricard C, Fernández M, Gastaldo J, et al. Short-term effects of synchrotron irradiation on vasculature and tissue in healthy mouse brain. J Synchrotron Radiat. 2009; 16:477–83. DOI: 10.1107/S0909049509015428 [PubMed: 19535860]

Ricard C, Fernandez M, Requardt H, et al. Synergistic effect of cisplatin and synchrotron irradiation on F98 gliomas growing in nude mice. J Synchrotron Radiat. 2013a; 20:777–84. DOI: 10.1107/S0909049513016567 [PubMed: 23955042]

Ricard C, Lamasse L, Jaouen A, et al. Combination of an optical parametric oscillator and quantum-dots 655 to improve imaging depth of vasculature by intravital multicolor two-photon microscopy. Biomed Opt Express. 2016a; 7:2362–72. DOI: 10.1364/BOE.7.002362 [PubMed: 27375951]

Ricard C, Stanchi F, Rodriguez T, et al. Dynamic quantitative intravital imaging of glioblastoma progression reveals a lack of correlation between tumor growth and blood vessel density. PLoS One. 2013b; 8:e72655.doi: 10.1371/journal.pone.0072655 [PubMed: 24069154]

Ricard C, Tchoghandjian A, Luche H, et al. Phenotypic dynamics of microglial and monocyte-derived cells in glioblastoma-bearing mice. Sci Rep. 2016b; 6:26381.doi: 10.1038/srep26381 [PubMed: 27193333]

Ricard C, Vacca B, Weber P. Three-dimensional imaging of small intestine morphology using non-linear optical microscopy and endogenous signals. J Anat. 2012; 221:279–83. DOI: 10.1111/j.1469-7580.2012.01529.x [PubMed: 22697278]

Ricard C, Vial J-C, Douady J, van der Sanden B. In vivo imaging of elastic fibers using sulforhodamine B. J Biomed Opt. 2007; 12:64017.doi: 10.1117/1.2821421

Rickgauer JP, Deisseroth K, Tank DW. Simultaneous cellular-resolution optical perturbation and imaging of place cell firing fields. Nat Neurosci. 2014; 17:1816–24. DOI: 10.1038/nn.3866 [PubMed: 25402854]

Rizzo MA, Springer G, Segawa K, et al. Optimization of pairings and detection conditions for measurement of FRET between cyan and yellow fluorescent proteins. Microsc Microanal. 2006; 12:238–54. DOI: 10.1017/S1431927606060235 [PubMed: 17481360]

Roder P, Hille C. ANG-2 for quantitative Na(+) determination in living cells by time-resolved fluorescence microscopy. Photochem Photobiol Sci. 2014; 13:1699–710. DOI: 10.1039/c4pp00061g [PubMed: 25311309]

Romanelli E, Sorbara CD, Nikić I, et al. Cellular, subcellular and functional in vivo labeling of the spinal cord using vital dyes. Nat Protoc. 2013; 8:481–90. DOI: 10.1038/nprot.2013.022 [PubMed: 23391891]

Ruthazer ES, Cline HT. Multiphoton Imaging of Neurons in Living Tissue: Acquisition and Analysis of Time-Lapse Morphological Data. Real-Time Imaging. 2002; 8:175–188. DOI: 10.1006/rtim.2002.0284

Sabatini BL, Oertner TG, Svoboda K. The life cycle of Ca(2+) ions in dendritic spines. Neuron. 2002; 33:439–52. [PubMed: 11832230]

Sadowski B, Kita H, Grzybowski M, et al. π-Expanded Dipyrrolonaphthyridinediones with Large Two-Photon Absorption Cross-Section Values. J Org Chem. 2017; doi: 10.1021/acs.joc.7b00831

Saito T, Nakatsuji N. Efficient gene transfer into the embryonic mouse brain using in vivo electroporation. Dev Biol. 2001; 240:237–246. [PubMed: 11784059]

Santisakultarm TP, Kersbergen CJ, Bandy DK, et al. Two-photon imaging of cerebral hemodynamics and neural activity in awake and anesthetized marmosets. J Neurosci Methods. 2016; 271:55–64. DOI: 10.1016/j.jneumeth.2016.07.003 [PubMed: 27393311]

Saria A, Lundberg JM. Evans blue fluorescence: quantitative and morphological evaluation of vascular permeability in animal tissues. J Neurosci Methods. 1983; 8:41–9. [PubMed: 6876872]

Sarkar P, Koushik SV, Vogel SS, et al. Photophysical properties of Cerulean and Venus fluorescent proteins. J Biomed Opt. 2009; 14:34047.doi: 10.1117/1.3156842

Schaffer CB, Friedman B, Nishimura N, et al. Two-photon imaging of cortical surface microvessels reveals a robust redistribution in blood flow after vascular occlusion. PLoS Biol. 2006; 4:e22.doi: 10.1371/journal.pbio.0040022 [PubMed: 16379497]

Schwarze T, Riemer J, Eidner S, Holdt H-J. A Highly K(+)-Selective Two-Photon Fluorescent Probe. Chemistry. 2015; 21:11306–10. DOI: 10.1002/chem.201501473 [PubMed: 26178764]

Senatorov VV, Stys PK, Hu B. Regulation of Na+,K+-ATPase by persistent sodium accumulation in adult rat thalamic neurones. J Physiol. 2000; 525(Pt 2):343–53. DOI: 10.1111/j.1469-7793.2000.00343.x [PubMed: 10835038]

Seo EW, Han JH, Heo CH, et al. A small-molecule two-photon probe for nitric oxide in living tissues. Chemistry. 2012; 18:12388–94. DOI: 10.1002/chem.201201197 [PubMed: 22907767]

Shaner NC, Campbell RE, Steinbach PA, et al. Improved monomeric red, orange and yellow fluorescent proteins derived from Discosoma sp. red fluorescent protein. Nat Biotechnol. 2004; 22:1567–72. DOI: 10.1038/nbt1037 [PubMed: 15558047]

Shaner NC, Lin MZ, McKeown MR, et al. Improving the photostability of bright monomeric orange and red fluorescent proteins. Nat Methods. 2008; 5:545–51. DOI: 10.1038/nmeth.1209 [PubMed: 18454154]

Shaner NC, Steinbach PA, Tsien RY. A guide to choosing fluorescent proteins. Nat Methods. 2005; 2:905–9. DOI: 10.1038/nmeth819 [PubMed: 16299475]

Shcherbo D, Merzlyak EM, Chepurnykh TV, et al. Bright far-red fluorescent protein for whole-body imaging. Nat Methods. 2007; 4:741–6. DOI: 10.1038/nmeth1083 [PubMed: 17721542]

Shcherbo D, Murphy CS, Ermakova GV, et al. Far-red fluorescent tags for protein imaging in living tissues. Biochem J. 2009; 418:567–74. DOI: 10.1042/BJ20081949 [PubMed: 19143658]

Shen Y, Dana H, Abdelfattah AS, et al. A genetically encoded Ca2+indicator based on circularly permutated sea anemone red fluorescent protein eqFP578. BMC Biol. 2018; 16:9.doi: 10.1186/s12915-018-0480-0 [PubMed: 29338710]

Shen Z, Lu Z, Chhatbar PY, et al. An artery-specific fluorescent dye for studying neurovascular coupling. Nat Methods. 2012; 9:273–6. DOI: 10.1038/nmeth.1857 [PubMed: 22266543]

Shi X, Li M, Zhao W, et al. Spectral imaging superlocalization microscopy for quantum dots. Sensors Actuators B Chem. 2015; 207:308–312. DOI: 10.1016/j.snb.2014.10.077

Shi X, Xie Z, Song Y, et al. Superlocalization spectral imaging microscopy of a multicolor quantum dot complex. Anal Chem. 2012; 84:1504–9. DOI: 10.1021/ac202784h [PubMed: 22304482]

Shigetomi E, Bushong EA, Haustein MD, et al. Imaging calcium microdomains within entire astrocyte territories and endfeet with GCaMPs expressed using adeno-associated viruses. J Gen Physiol. 2013; 141:633–47. DOI: 10.1085/jgp.201210949 [PubMed: 23589582]

Shigetomi E, Patel S, Khakh BS. Probing the Complexities of Astrocyte Calcium Signaling. Trends Cell Biol. 2016; 26:300–12. DOI: 10.1016/j.tcb.2016.01.003 [PubMed: 26896246]

Shoham D, Glaser DE, Arieli A, et al. Imaging cortical dynamics at high spatial and temporal resolution with novel blue voltage-sensitive dyes. Neuron. 1999; 24:791–802. [PubMed: 10624943]

Siegel MS, Isacoff EY. A genetically encoded optical probe of membrane voltage. Neuron. 1997; 19:735–41. [PubMed: 9354320]

Singh H, Lee HW, Heo CH, et al. A Golgi-localized two-photon probe for imaging zinc ions. Chem Commun (Camb). 2015; 51:12099–102. DOI: 10.1039/c5cc03884g [PubMed: 26121157]

Smith PG, Baldacchini T, Carter J, Zadoyan R. TWO-PHOTON MICROSCOPY/MULTIMODAL IMAGING: Femtosecond laser developments advance two-photon imaging. BioOptics World. 2012. http://www.bioopticsworld.com/articles/print/volume-5/issue-04/features/femtosecond-laser-developments-advance-two-photon-imaging.html. Accessed 1 Jan 2017

So PT, Dong CY, Masters BR, Berland KM. Two-photon excitation fluorescence microscopy. Annu Rev Biomed Eng. 2000; 2:399–429. DOI: 10.1146/annurev.bioeng.2.1.399 [PubMed: 11701518]

Son JH, Lim CS, Han JH, et al. Two-photon Lysotrackers for in vivo imaging. J Org Chem. 2011; 76:8113–6. DOI: 10.1021/jo201504h [PubMed: 21838289]

Srinivasan R, Huang BS, Venugopal S, et al. Ca2+ signaling in astrocytes from Ip3r2−/− mice in brain slices and during startle responses in vivo. 2015; doi: 10.1038/nn.4001

St-Pierre F, Marshall JD, Yang Y, et al. High-fidelity optical reporting of neuronal electrical activity with an ultrafast fluorescent voltage sensor. Nat Neurosci. 2014; 17:884–9. DOI: 10.1038/nn.3709 [PubMed: 24755780]

Stringari C, Abdeladim L, Malkinson G, et al. Multicolor two-photon imaging of endogenous fluorophores in living tissues by wavelength mixing. Sci Rep. 2017; 7:3792.doi: 10.1038/s41598-017-03359-8 [PubMed: 28630487]

Stringari C, Nourse JL, Flanagan LA, Gratton E. Phasor fluorescence lifetime microscopy of free and protein-bound NADH reveals neural stem cell differentiation potential. PLoS One. 2012; 7:e48014.doi: 10.1371/journal.pone.0048014 [PubMed: 23144844]

Svoboda K, Yasuda R. Principles of two-photon excitation microscopy and its applications to neuroscience. Neuron. 2006; 50:823–39. DOI: 10.1016/j.neuron.2006.05.019 [PubMed: 16772166]

Swirski FK, Berger CR, Figueiredo J-L, et al. A near-infrared cell tracker reagent for multiscopic in vivo imaging and quantification of leukocyte immune responses. PLoS One. 2007; 2:e1075.doi: 10.1371/journal.pone.0001075 [PubMed: 17957257]

Tabata H, Nakajima K. Efficient in utero gene transfer system to the developing mouse brain using electroporation: visualization of neuronal migration in the developing cortex. Neuroscience. 2001; 103:865–872. DOI: 10.1016/S0306-4522(01)00016-1 [PubMed: 11301197]

Takahashi M, Sato K, Nomura T, Osumi N. Manipulating gene expressions by electroporation in the developing brain of mammalian embryos. Differentiation. 2002; 70:155–162. DOI: 10.1046/j.1432-0436.2002.700405.x [PubMed: 12147135]

Takaki M, Goto K, Kawahara I, Nabekura J. Activation of 5-HT4 receptors facilitates neurogenesis of injured enteric neurons at an anastomosis in the lower gut. J Smooth Muscle Res. 2015; 51:82–94. DOI: 10.1540/jsmr.51.82 [PubMed: 26658112]

Takiguchi-Hayashi K, Sekiguchi M, Ashigaki S, et al. Generation of reelin-positive marginal zone cells from the caudomedial wall of telencephalic vesicles. J Neurosci. 2004; 24:2286–2295. [PubMed: 14999079]

Tallini YN, Ohkura M, Choi B-R, et al. Imaging cellular signals in the heart in vivo: Cardiac expression of the high-signal Ca2+ indicator GCaMP2. Proc Natl Acad Sci U S A. 2006; 103:4753–8. DOI: 10.1073/pnas.0509378103 [PubMed: 16537386]

Tervo DGR, Hwang B-Y, Viswanathan S, et al. A Designer AAV Variant Permits Efficient Retrograde Access to Projection Neurons. Neuron. 2016; 92:372–382. DOI: 10.1016/j.neuron.2016.09.021 [PubMed: 27720486]

Thaler C, Vogel SS. Quantitative linear unmixing of CFP and YFP from spectral images acquired with two-photon excitation. Cytometry A. 2006; 69:904–11. DOI: 10.1002/cyto.a.20267 [PubMed: 16888770]

Tischbirek C, Birkner A, Jia H, et al. Deep two-photon brain imaging with a red-shifted fluorometric Ca2+ indicator. Proc Natl Acad Sci U S A. 2015; 112:11377–82. DOI: 10.1073/pnas.1514209112 [PubMed: 26305966]

Tozer GM, Ameer-Beg SM, Baker J, et al. Intravital imaging of tumour vascular networks using multi-photon fluorescence microscopy. Adv Drug Deliv Rev. 2005; 57:135–52. DOI: 10.1016/j.addr.2004.07.015 [PubMed: 15518926]

Trägårdh J, Robb G, Amor R, et al. Exploration of the two-photon excitation spectrum of fluorescent dyes at wavelengths below the range of the Ti:Sapphire laser. J Microsc. 2015; 259:210–8. DOI: 10.1111/jmi.12255 [PubMed: 25946127]

Tran CHT, Gordon GR. Astrocyte and microvascular imaging in awake animals using two-photon microscopy. Microcirculation. 2015; 22:219–27. DOI: 10.1111/micc.12188 [PubMed: 25582833]

Tsien RY, Rink TJ, Poenie M. Measurement of cytosolic free Ca2+ in individual small cells using fluorescence microscopy with dual excitation wavelengths. Cell Calcium. 1985; 6:145–157. DOI: 10.1016/0143-4160(85)90041-7 [PubMed: 3874696]

Vadakkan TJ, Culver JC, Gao L, et al. Peak Multiphoton Excitation of mCherry Using an Optical Parametric Oscillator (OPO). J Fluoresc. 2009; 19:1103–1109. DOI: 10.1007/s10895-009-0510-y [PubMed: 19590939]

Velasco MGM, Allgeyer ES, Yuan P, et al. Absolute two-photon excitation spectra of red and far-red fluorescent probes. Opt Lett. 2015; 40:4915–8. [PubMed: 26512482]

Vérant P, Ricard C, Serduc R, et al. In vivo staining of neocortical astrocytes via the cerebral microcirculation using sulforhodamine B. J Biomed Opt. 2013; 13:64028.doi: 10.1117/1.3041163

Wallace DJ. The use of quinacrine (Atabrine) in rheumatic diseases: a reexamination. Semin Arthritis Rheum. 1989; 18:282–96. [PubMed: 2658071]

Wang C, Mei L. In utero electroporation in mice. Methods Mol Biol. 2013; 1018:151–63. DOI: 10.1007/978-1-62703-444-9_15 [PubMed: 23681626]

Wang C, Yeh AT. Two-photon excited fluorescence enhancement with broadband versus tunable femtosecond laser pulse excitation. J Biomed Opt. 2012; 17:25003.doi: 10.1117/1.JBO.17.2.025003

Wang F, Qi LS. Applications of CRISPR Genome Engineering in Cell Biology. Trends Cell Biol. 2016; 26:875–888. DOI: 10.1016/j.tcb.2016.08.004 [PubMed: 27599850]

Wang K, Sun W, Richie CT, et al. Direct wavefront sensing for high-resolution in vivo imaging in scattering tissue. Nat Commun. 2015; 6:7276.doi: 10.1038/ncomms8276 [PubMed: 26073070]

Weigelin B, Bakker G-J, Friedl P. Third harmonic generation microscopy of cells and tissue organization. J Cell Sci. 2016; 129:245–55. DOI: 10.1242/jcs.152272 [PubMed: 26743082]

Weissman TA, Pan YA. Brainbow: new resources and emerging biological applications for multicolor genetic labeling and analysis. Genetics. 2015; 199:293–306. DOI: 10.1534/genetics.114.172510 [PubMed: 25657347]

Wickersham IR, Lyon DC, Barnard RJO, et al. Monosynaptic restriction of transsynaptic tracing from single, genetically targeted neurons. Neuron. 2007; 53:639–47. DOI: 10.1016/j.neuron.2007.01.033 [PubMed: 17329205]

Williams RM, Zipfel WR, Webb WW. Interpreting second-harmonic generation images of collagen I fibrils. Biophys J. 2005; 88:1377–86. DOI: 10.1529/biophysj.104.047308 [PubMed: 15533922]

Witte S, Negrean A, Lodder JC, et al. Label-free live brain imaging and targeted patching with third-harmonic generation microscopy. Proc Natl Acad Sci U S A. 2011; 108:5970–5. DOI: 10.1073/pnas.1018743108 [PubMed: 21444784]

Woodard LE, Wilson MH. piggyBac-ing models and new therapeutic strategies. Trends Biotechnol. 2015; 33:525–33. DOI: 10.1016/j.tibtech.2015.06.009 [PubMed: 26211958]

Xu C, Webb WW. Measurement of two-photon excitation cross sections of molecular fluorophores with data from 690 to 1050 nm. J Opt Soc Am B. 1996; 13:481.doi: 10.1364/JOSAB.13.000481

Xu Y, Zou P, Cohen AE. Voltage imaging with genetically encoded indicators. Curr Opin Chem Biol. 2017; 39:1–10. DOI: 10.1016/j.cbpa.2017.04.005 [PubMed: 28460291]

Yan P, Acker CD, Zhou W-L, et al. Palette of fluorinated voltage-sensitive hemicyanine dyes. Proc Natl Acad Sci U S A. 2012; 109:20443–8. DOI: 10.1073/pnas.1214850109 [PubMed: 23169660]

Yang G, Pan F, Parkhurst CN, et al. Thinned-skull cranial window technique for long-term imaging of the cortex in live mice. Nat Protoc. 2010; 5:201–8. DOI: 10.1038/nprot.2009.222 [PubMed: 20134419]

Yasuda R, Harvey CD, Zhong H, et al. Supersensitive Ras activation in dendrites and spines revealed by two-photon fluorescence lifetime imaging. Nat Neurosci. 2006; 9:283–291. DOI: 10.1038/nn1635 [PubMed: 16429133]

Yasuda R, Nimchinsky EA, Scheuss V, et al. Imaging calcium concentration dynamics in small neuronal compartments. Sci STKE. 2004; 2004:pl5.doi: 10.1126/stke.2192004pl5 [PubMed: 14872098]

Yi KD, Covey DF, Simpkins JW. Mechanism of okadaic acid-induced neuronal death and the effect of estrogens. J Neurochem. 2009; 108:732–40. DOI: 10.1111/j.1471-4159.2008.05805.x [PubMed: 19054278]

Yin H, Zhang B, Yu H, et al. Two-photon fluorescent probes for biological Mg(2+). detection based on 7-substituted coumarin. J Org Chem. 2015; 80:4306–12. DOI: 10.1021/jo502775t [PubMed: 25844880]

Yu H, Senarathna J, Tyler BM, et al. Miniaturized optical neuroimaging in unrestrained animals. Neuroimage. 2015; 113:397–406. DOI: 10.1016/j.neuroimage.2015.02.070 [PubMed: 25791782]

Yuste R, MacLean J, Vogelstein J, Paninski L. Imaging Action Potentials with Calcium Indicators. Cold Spring Harb Protoc. 2011; 2011 pdb.prot5650-prot5650. doi: 10.1101/pdb.prot5650

Zapata-Hommer O, Griesbeck O. Efficiently folding and circularly permuted variants of the Sapphire mutant of GFP. BMC Biotechnol. 2003; 3:5.doi: 10.1186/1472-6750-3-5 [PubMed: 12769828]

Zariwala HA, Borghuis BG, Hoogland TM, et al. A Cre-dependent GCaMP3 reporter mouse for neuronal imaging in vivo. J Neurosci. 2012; 32:3131–41. DOI: 10.1523/JNEUROSCI.4469-11.2012 [PubMed: 22378886]

Zehentbauer FM, Moretto C, Stephen R, et al. Fluorescence spectroscopy of Rhodamine 6G: concentration and solvent effects. Spectrochim Acta A Mol Biomol Spectrosc. 2014; 121:147–51. DOI: 10.1016/j.saa.2013.10.062 [PubMed: 24239710]

Zhang H, Liu J, Wang L, et al. Amino-Si-rhodamines: A new class of two-photon fluorescent dyes with intrinsic targeting ability for lysosomes. Biomaterials. 2018; 158:10–22. DOI: 10.1016/j.biomaterials.2017.12.013 [PubMed: 29272765]

Zhou W-L, Yan P, Wuskell JP, et al. Intracellular long-wavelength voltage-sensitive dyes for studying the dynamics of action potentials in axons and thin dendrites. J Neurosci Methods. 2007; 164:225–39. DOI: 10.1016/j.jneumeth.2007.05.002 [PubMed: 17560661]

Zhu H, Derksen R, Krause C, et al. Fluorescent Intensity of Dye Solutions under Different pH Conditions. J ASTM Int. 2005; 2:12926.doi: 10.1520/JAI12926

Zhu J-Y, Zhou L-F, Li Y-K, et al. In vivo near-infrared fluorescence imaging of amyloid-β plaques with a dicyanoisophorone-based probe. Anal Chim Acta. 2017; 961:112–118. DOI: 10.1016/j.aca.2017.01.017 [PubMed: 28224903]

Zimmermann T, Marrison J, Hogg K, O'Toole P. Clearing up the signal: spectral imaging and linear unmixing in fluorescence microscopy. Methods Mol Biol. 2014; 1075:129–48. DOI: 10.1007/978-1-60761-847-8_5 [PubMed: 24052349]

Zimmermann T, Rietdorf J, Girod A, et al. Spectral imaging and linear un-mixing enables improved FRET efficiency with a novel GFP2-YFP FRET pair. FEBS Lett. 2002; 531:245–9. [PubMed: 12417320]

Zinselmeyer BH, Dempster J, Wokosin DL, et al. Chapter 16. Two-photon microscopy and multidimensional analysis of cell dynamics. Methods Enzymol. 2009; 461:349–78. DOI: 10.1016/S0076-6879(09)05416-0 [PubMed: 19480927]

Zipfel WR, Williams RM, Christie R, et al. Live tissue intrinsic emission microscopy using multiphoton-excited native fluorescence and second harmonic generation. Proc Natl Acad Sci U S A. 2003a; 100:7075–80. DOI: 10.1073/pnas.0832308100 [PubMed: 12756303]

Zipfel WR, Williams RM, Webb WW. Nonlinear magic: multiphoton microscopy in the biosciences. Nat Biotechnol. 2003b; 21:1369–77. DOI: 10.1038/nbt899 [PubMed: 14595365]

Zong W, Wu R, Li M, et al. Fast high-resolution miniature two-photon microscopy for brain imaging in freely behaving mice. Nat Methods. 2017; doi: 10.1038/nmeth.4305

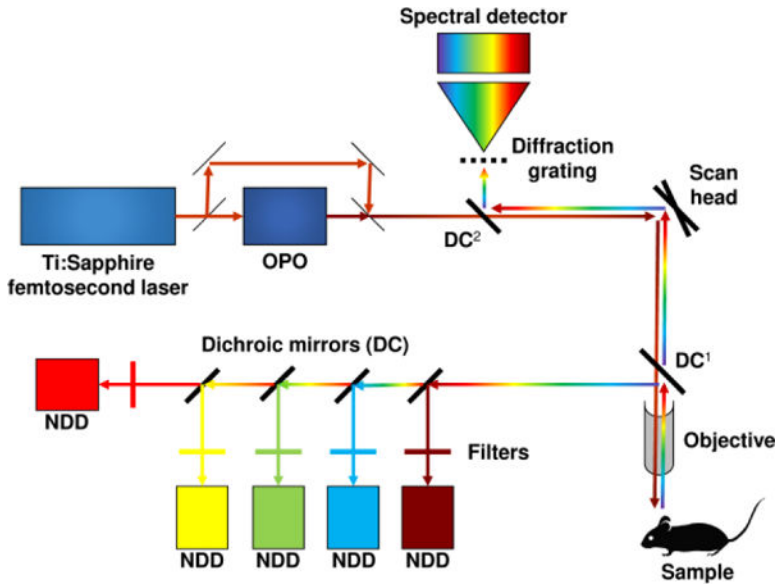

Fig. 1.

Optical setup for multicolor two-photon microscopy

DC: dichroic mirror; NDD: non-descanned detector; OPO: optical parametric oscillator.

[1]: Dichroic mirror used to collect fluorescent photons on five non-descanned detectors. Excitatory infrared photons pass through the mirror whereas fluorescence photons are reflected. This mirror must be removed to collect photons in descanned mode.

[2]: Dichroic mirror used to collect fluorescent photons on a spectral chip in descanned mode.

Modified from (Ricard and Debarbieux 2014).

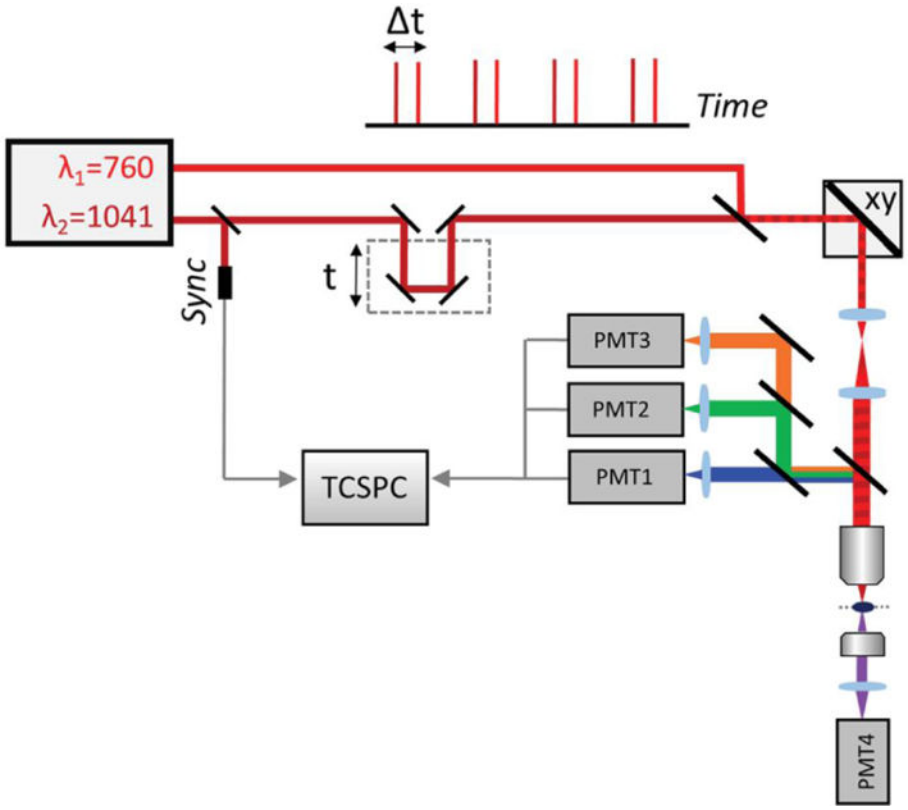

Fig. 2.

Wavelength mixing–fluorescence lifetime imaging of endogenous fluorophores When the excitation beams λ_1 = 760 nm and λ_2 = 1041 nm are synchronized (Δt = 0), a third virtual wavelength for two-photon excitation λ_v = 879 nm is created by wavelength mixing. A time-correlated single photon counting system (TCSPC) is used to perform FLIM. Originally published in *Scientific reports* (Stringari et al. 2017) under a Creative Commons Attribution 4.0 International License (http://creativecommons.org/licenses/by/4.0/).

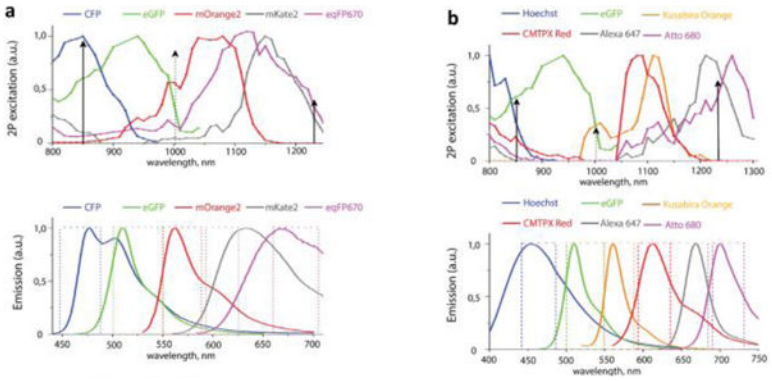

Fig. 3.

Wavelength-mixing optimal combination of two sets of fluorophores Two-photon excitation and emission spectra of two sets of fluorophores that can be efficiently excited by wavelength mixing with λ_1 = 850 nm and λ_2 = 1230 nm (full arrows), resulting in λ_v = 1005 nm (dashed arrow). (a) **CFP**, **eGFP**, **mOrange2**, **mKate2**, **eqFP670**. (b) **Hoechst**, **eGFP**, **Kusabira Orange**, **CMTPX Red**, **Alexa 647**, **Atto 680**. Originally published in *Scientific reports* (Rakhymzhan et al. 2017) under a Creative Commons Attribution 4.0 International License (http://creativecommons.org/licenses/by/4.0/).

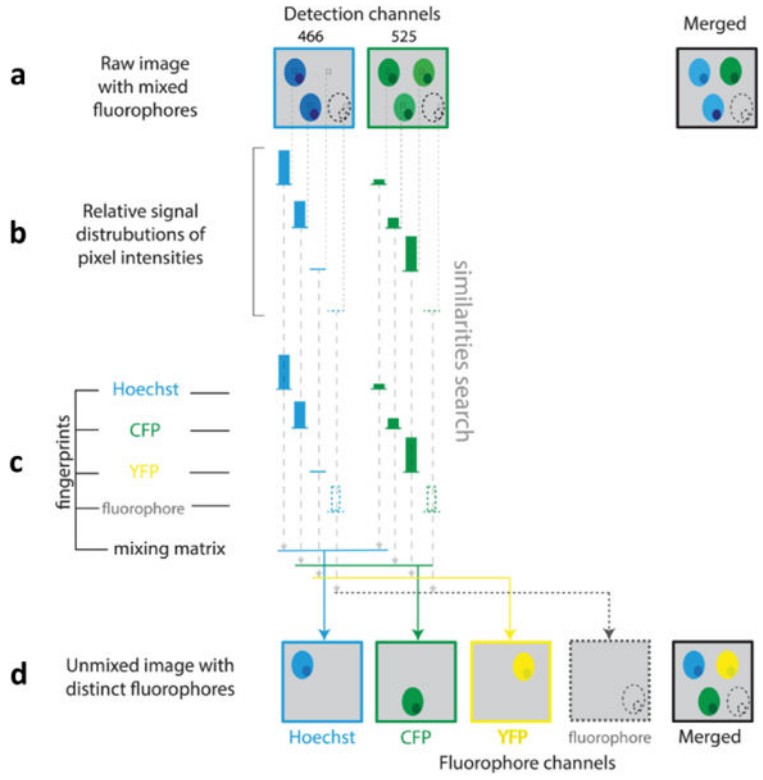

Fig. 4.

Example of similarity unmixing of more fluorochromes than available channels (a) Images of cells labelled with several fluorophores, showing crosstalk in two detection channels. (b) Extraction of a relative signal distribution in the two channels pixels by pixel. (c) The algorithm calculates similarities between the known fingerprints of each fluorophore and the signature of undefined fluorophores extracted during step (b). (d) Color separation based on the ratios between the fluorophore fingerprints. Originally published in *Scientific reports* (Rakhymzhan et al. 2017) under a Creative Commons Attribution 4.0 International License (http://creativecommons.org/licenses/by/4.0/).

Table 1

Routes of administration of fluorochromes for intravital two-photon microscopy of brain cells, structures, and functions.

Technique	Target	Probe
Single-cell electroporation	*Diverse* (*e.g.* neurons (Liu and Haas 2011))	*Diverse*
In utero electroporation (Wang and Mei 2013)	*e.g.* layer 2/3 cortical neurons (Saito and Nakatsuji 2001)	*e.g.* **eGFP**
Intraperitoneal administration	Amyloid-β plaques	*e.g.* **SAD1** (Heo et al. 2013)
Intravenous administration	Astrocytes	**Sulforhodamine 101** (Nimmerjahn et al. 2004), **sulforhodamine B** (Vérant et al. 2013)
	Blood vessels	*e.g.* **Rhodamine B** dextran, **quantum-dots** (Ricard et al. 2016a)
	Arteries	**Alexa Fluor 633** (Shen et al. 2012)
	Amyloid-β plaques	*e.g.* **DCIP-1** (Zhu et al. 2017)
Viral transduction (Nassi et al. 2015)	Spatially-restricted (*e.g.* axonal domain of neurons (Tervo et al. 2016)) and genetically-defined cells (*e.g.* oligodendrocytes (Powell et al. 2016))	*Diverse*
	Calcium activity	Genetically encoded Ca^{2+} indicators (GECIs)
	Membrane potential (V_m)	Genetically encoded voltage sensors (GEVs)
Whole-cell and bulk loading	Ion activity (neurons, astrocytes (Reeves et al. 2011))	Ion indicators (*e.g.* **Fura-2-AM**, **Fluo-4-AM**, **Oregon Green BAPTA-1** (Garaschuk et al. 2006))
	Membrane potential (V_m)	Voltage-sensitive dyes (*e.g.* **ANNINE-6** (Kuhn et al. 2008), **RH-1692** (Murphy et al. 2008))

Table 2

Biophysical properties of two-photon–suitable non-specific probes : peak wavelength of two-photon action cross-section (λ_{2PA}) ; peak two-photon action cross-section ($\sigma_2\varphi$) ; peak wavelength of molecular brightness ($\lambda_{\varepsilon\_max}$) ; peak molecular brightness (ε_{max}) ; fluorescence wavelength (λ_{fluo}). Probes discussed in the text are in bold.

Probe	**λ_{2PA} [nm]**	**$\sigma_2\varphi$ [GM]**	**$\lambda_{\varepsilon\ max}$ [nm]**	**ε_{max} [kcps m]**	**λ_{fluo} [nm]**	**Comment**	**Reference**
— Pond 2002 Derivative 1	830	1207[a]			536	Hydropho bic	Figure 3(1) in (Pond et al. 2002)
— Pond 2002 Derivative 2	830	1427[a]			528	Hydropho bic	Figure 3(2) in (Pond et al. 2002)
— Pond 2002 Derivative 3	790	2.67[a]			504	Hydropho bic	Figure 3(3) in (Pond et al. 2002)
— Pond 2002 Derivative 4	825	11[a]			510	Hydropho bic	Figure 3(4) in (Pond et al. 2002)
— Sadowski 2017 Derivative 4a	740	112			671		Figure 3 in (Sadowski et al. 2017)
— Sadowski 2017 Derivative 4b	820	83			699		Figure 3 in (Sadowski et al. 2017)
— Sadowski 2017 Derivative 4c	740	70			662		Figure 3 in (Sadowski et al. 2017)
— Sadowski 2017 Derivative 5a (7a)	720	1450			633		Figure 3 in (Sadowski et al. 2017)
— Sadowski 2017 Derivative 5b (7c)	720	500			643		Figure 3 in (Sadowski et al. 2017)
— Sadowski 2017 Derivative 5c (7d)	860	340			736		Figure 3 in (Sadowski et al. 2017)
5C-TMR	830	135	850	31.5	580[b]		Figure 5 in (Mütze et al. 2012)
7-amino-4- methylcoumarin	703 < 722 >> 863				439[b]		Figure 3 in (Bestvater et al. 2002)
Alexa Fluor 350	~715				442[b]		Figure 5C in (Trägårdh et al. 2015)
Alexa Fluor 430	870	11.6	910	16	541[b]		Figure 2 in (Mütze et al. 2012)
Alexa Fluor 488	940	~30			519[b]		Figure 2 in (Anderson and Webb 2011)
Alexa Fluor 514			790, 960	~32, ~25	542[b]		Figure 2 in (Mütze et al. 2012)
Alexa Fluor 546			820	58	573[b]		Figure 2 in (Mütze et al. 2012)

Probe	λ_{2PA} [nm]	$\sigma_2\varphi$ [GM]	$\lambda_{e\ max}$ [nm]	ε_{max} [kcps m]	λ_{fluo} [nm]	Comment	Reference
Alexa Fluor 568			780	~25	603[b]		Figure 2 in (Mütze et al. 2012)
Alexa Fluor 594			800	~32	617[b]		Figure 2 in (Mütze et al. 2012)
Alexa Fluor 610			820	~28	628[b]		Figure 2 in (Mütze et al. 2012)
Alexa Fluor 633			820	~24	647[b]	Arteries (Shen et al. 2012)	Figure 2 in (Mütze et al. 2012)
Alexa Fluor 647	1240	~45			665[b]	OPO- friendly	Figure 7 in (Kobat et al. 2009)
Alexa Fluor 680	1280	~75			702[b]	OPO- friendly	Figure 7 in (Kobat et al. 2009)
Alexa Fluor 700	1300	~52			723[b]	OPO- friendly	Figure 7 in (Kobat et al. 2009)
Aminomethyl coumarin acetate	700				445[b]		– (Bok et al. 2015)
Ant-PHEA (in water)	800	2480			575[b]		Figure 6 in (Mettra et al. 2016)
ATTO 590	790	~250 (NHS ester)			624[b]	STED- compatibl e	Figure 2E in (Velasco et al. 2015)
ATTO 594	800	~220 (NHS ester), ~140 (antibodie s)			627[b]	STED- compatibl e	Figure 2D in (Velasco et al. 2015)
ATTO 647N	840	~270 (NHS ester), ~120 (streptavid in)			669[b]	STED- compatibl e	Figure 2A in (Velasco et al. 2015)
ATTO 680	~1260				695[b]	OPO- friendly	Figure 2D in (Rakhymzha n et al. 2017)
BODIPY (in water)	920	17.12			Variable		*
BODIPY 492/515 (in water)	920	14.3	920	47.4	515		Figure 5 in (Mütze et al. 2012)
BODIPY-FL (in DMSO)	920 << 972				512[b]		Figure 3 in (Bestvater et al. 2002)
BODIPY-TR	1080	242	106 0	15.2	618[b]		Figure 5 in (Mütze et al. 2012)
Brilliant Violet 421	710- 1000				421		– (Figure 6) (Chattopadhyay et al. 2012)
Cascade Blue	740, 800	2.1 (at 750 nm)			420[b]		Figure 7 in (Xu and Webb 1996)
CellTracker Blue	780				466[b]		– (Zinselmeye r et al. 2009)
CellTracker Orange	820				565[b]		– (Miller et al. 2002)
CellTracker Red	~1080				602[b]		Figure 2D in (Rakhymzha n et al. 2017)

Probe	λ_{2PA} [nm]	$\sigma_2\varphi$ [GM]	$\lambda_{e\ max}$ [nm]	ε_{max} [kcps m]	λ_{fluo} [nm]	Comment	Reference
CFP	840	~180			485[b]		Figure 3B in (Zipfel et al. 2003b)
CFSE	780				521[b]		– (Miller et al. 2002)
Citrine	968	6.7			529 (Griesbeck et al. 2001)		Figure 1 in (Drobizhev et al. 2011)
Coumarin 307	800	15.3			490 (in ethanol)[b]		*
Cy2-IgG	837 < 905 > 981				505[b]		Figure 4 in (Bestvater et al. 2002)
Cy3-IgG	1032				565[b]		Figure 4 in (Bestvater et al. 2002)
Cy5.5	1280	~60			702[b]	OPO- friendly	Figure 7 in (Kobat et al. 2009)
Dronpa-3	920				515	Reversibl y switchable	– (Ando et al. 2007; Kao et al. 2012)
dsRed	> 990	108			583 (Shaner et al. 2008)		*
dsRed2	1050	73			587		Figure S1 in (Drobizhev et al. 2011)
E2-Crimson	1138	1.8			643		Figure S1 in (Drobizhev et al. 2011)
EBFP2.0	750	9.2			446		Figure 1 in (Drobizhev et al. 2011)
eCFP	857	12			476		Figure S1 in (Drobizhev et al. 2011)
eGFP (pH 8)	927	30			510		Figure S1 in (Drobizhev et al. 2011)
eqFP650	1112	8.5			646		Figure S1 in (Drobizhev et al. 2011)
eqFP670	1120	1.3			661		Figure S1 in (Drobizhev et al. 2011)
Evans Blue	850				680 (Saria and Lundberg 1983)		– (Bennewitz et al. 2014)
eYFP	960	25			527 (Merzlyak et al. 2007)		– (Table 2) (Blab et al. 2001)
Fluorescein (in water, pH = 11)	770	39	800	18.4	520 (Zhu et al. 2005)		Figure 5 in (Mütze et al. 2012)
Fluorescein isiothiocyanate (FITC)	800				525[b]		Figure 3B in (Wang and Yeh 2012)

Brain Struct Funct. Author manuscript; available in PMC 2019 September 01.

Probe	λ_{2PA} [nm]	$\sigma_2\varphi$ [GM]	$\lambda_{e\ max}$ [nm]	ε_{max} [kcps m]	λ_{fluo} [nm]	Comment	Reference
GFP	800	6.5			504 (Chattoraj et al. 1996)		*
Hilyte Fluor 488	~815, 960	~55, ~30			525[b]		Figure 2 in (Anderson and Webb 2011)
Katushka	1080	23			635 (Shcherbo et al. 2007)		Figure S1 in (Drobizhev et al. 2011)
Katushka2	1140	27			633[b]	OPO- friendly	Figure S1 in (Drobizhev et al. 2011)
Kusabira Orange	~1110				561 (Karasawa et al. 2004)		Figure 2D in (Rakhymzhan et al. 2017)
Lissamine rhodamine	837 >> 1116				~580[b]		Figure 4 in (Bestvater et al. 2002)
LSS-mKate1	920	~40			624		Figure 1E in (Piatkevich et al. 2010)
LSS-mKate2	920	~90			605		Figure 1E in (Piatkevich et al. 2010)
Lucifer Yellow	840	1.4			540[b]		*
mAmetrine	809	40			526 (Ai et al. 2008)		Figure S1 in (Drobizhev et al. 2011)
mBanana	1070	44			553 (Shaner et al. 2004)	OPO- friendly	Figure S1 in (Drobizhev et al. 2011)
mCardinal	>1080				659	OPO- friendly	Figure S3 in (Chu et al. 2014)
mCerulean	840	~75			475-503 (Ai et al. 2006)		Figure S1 in (Drobizhev et al. 2011)
mCFP	840	187			475 (Shaner et al. 2005)		*
mCherry	1080 (Drobizhev et al. 2011), 1160 (Vadakkan et al. 2009)	6.4 (at 1080 nm)			610 (Shaner et al. 2008)	OPO- friendly	Figure S1 in (Drobizhev et al. 2011) and Figure 8 in (Vadakkan et al. 2009)
mCitrene	960	~320					Figure 3C in (Rizzo et al. 2006)
mCitrine (pH 8)	950	7.6			527		Figure S1 in (Drobizhev et al. 2011)
mEGFP	960	~300			507 (Shaner et al. 2005)		Figure 3B in (Rizzo et al. 2006)

Brain Struct Funct. Author manuscript; available in PMC 2019 September 01.

Probe	λ_{2PA} [nm]	$\sigma_2\varphi$ [GM]	$\lambda_{e\ max}$ [nm]	ε_{max} [kcps m]	λ_{fluo} [nm]	Comment	Reference
mGrape3	1140	1.6			645		Figure S1 in (Drobizhev et al. 2011)
mKate (pH 8)	1118	14			635 (Shcherbo et al. 2007)	OPO- friendly	Figure S1 in (Drobizhev et al. 2011)
mKate2	1140	30			633 (Shcherbo et al. 2009)	OPO- friendly	Figure S1 in (Drobizhev et al. 2011)
mKeima	~880	~70			620		Figure 1E in (Piatkevich et al. 2010)
mNeptune	1104	12			651 (Chu et al. 2014)	OPO- friendly	Figure S1 in (Drobizhev et al. 2011)
mOrange	1080	47			565	OPO- friendly	Figure S1 in (Drobizhev et al. 2011)
mOrange2	~1080				565 (Shaner et al. 2008)		Figure 2B in (Rakhymzhan et al. 2017)
mPlum	1105	2.9			644		Figure S1 in (Drobizhev et al. 2011)
mRaspberry	1118	5.8			625 (Shcherbo et al. 2007)	OPO- friendly	Figure S1 in (Drobizhev et al. 2011)
mRFP	1080	13			611		Figure S1 in (Drobizhev et al. 2011)
mStrawberry	1070	6.8			596 (Shaner et al. 2004)		Figure S1 in (Drobizhev et al. 2011)
mTangerine	1055	3.3			584		Figure S1 in (Drobizhev et al. 2009, 2011)
mVenus	960	~200			525 (Sarkar et al. 2009)		Figure 3C in (Rizzo et al. 2006)
mWasabi	927	7.3			508		Figure S1 in (Drobizhev et al. 2011)
Near-iRFP	1260				713	OPO- friendly	Figure S5 in (Filonov et al. 2011)
Neptune	1120	16			647		Figure S1 in (Drobizhev et al. 2011)
Pacific Blue	780				455[b]		– (Lukomska et al. 2006)
Peridinin chlorophyll	850				678		– (Bok et al. 2015)
Phycoerythrin	1064	322			576[b]		– (Chen et al. 1997; So et al. 2000)

Brain Struct Funct. Author manuscript; available in PMC 2019 September 01.

Probe	λ_{2PA} [nm]	$\sigma_2\varphi$ [GM]	$\lambda_{e\ max}$ [nm]	ε_{max} [kcps m]	λ_{fluo} [nm]	Comment	Reference
QD550 (organic)	700- 1000	~2000			550	Broad absorption spectrum	Figure 1A in (Larson et al. 2003)
QD550 (water- soluble)	700- 1000	~2000			550	Broad absorption spectrum	Figure 1A in (Larson et al. 2003)
QD567 (water- soluble)	700- 1000	~10000			567	Broad absorption spectrum	Figure 1A in (Larson et al. 2003)
QD605 (water- soluble)	700- 1000	47000			605	Broad absorption spectrum	Figure 1A in (Larson et al. 2003)
QD630 (organic)	700- 1000	~2000			630	Broad absorption spectrum	Figure 1A in (Larson et al. 2003)
Resorufin	1040	9	106 0	33.9	585[b]		Figure 5 in (Mütze et al. 2012)
Rhodamine 110	790	48	800	30.9	521[b]		Figure 5 in (Mütze et al. 2012)
Rhodamine 6G	700, ~820	~150, ~40			~570 (Zehentbauer et al. 2014)		Figure 1C in (Albota et al. 1998)
Rhodamine B	830	204			590[b]		*
Rhodamine Green	850				527[b]		Figure 3 in (Heinze et al. 2000)
Sapphire	810	40			511 (Zapata-Hommer and Griesbeck 2003)		*
SeTa-632	820	200			641[b]	Broad absorption spectrum	Figure 1B in (Podgorski et al. 2012)
SeTa-646	840	500			656[b]	Broad absorption spectrum	Figure 1B in (Podgorski et al. 2012)
SeTa-660	840	1500			672[b]	Broad absorption spectrum	Figure 1B in (Podgorski et al. 2012)
SeTa-670	840	2000			688[b]	Broad absorption spectrum	Figure 1B in (Podgorski et al. 2012)
SeTa-700	900	200			703[b]	Broad absorption spectrum	Figure 1B in (Podgorski et al. 2012)
SeTau-647	920	3000			694[b]	Broad absorption spectrum	Figure 2A in (Podgorski et al. 2012)
SeTau-665	900	9000			712[b]	Broad absorption spectrum	Figure 1B in (Podgorski et al. 2012)
Silicon Rhodamine	830	~140 (antibodie s)			~670	STED- compatibl e	Figure 2B in (Velasco et al. 2015)

Brain Struct Funct. Author manuscript; available in PMC 2019 September 01.

Probe	λ_{2PA} [nm]	$\sigma_2\varphi$ [GM]	$\lambda_{e\ max}$ [nm]	ε_{max} [kcps m]	λ_{fluo} [nm]	Comment	Reference
STAR 635P	820	~110 (NHS carbonate)			651[b]	STED- compatibl e	Figure 2C in (Velasco et al. 2015)
TagGFP2	896	27			506[b]		Figure S1 in (Drobizhev et al. 2011)
TagRFP	1050	42			584 (Shaner et al. 2008)		Figure S1 in (Drobizhev et al. 2011)
tdKatushka2	1100	63			633 (Shcherbo et al. 2009)	OPO- friendly	Figure S1 in (Drobizhev et al. 2011)
tdRFP	1110	13.7[a]			579	OPO- friendly	Figure 2B in (Herz et al. 2010)
tdTomato	1050	200			581 (Shaner et al. 2008)	OPO- friendly	Figure S1 in (Drobizhev et al. 2011)
Tetramethylrhoda mine (TRITC)	840				576[b]		Figure 3C in (Wang and Yeh 2012)
Texas Red	780				615 (Cahalan et al. 2002)		Figure 3 in (Heinze et al. 2000)
Venus	~965, ~1015	~19, ~15			528 (Nagai et al. 2002)		Figure 7B in (Hashimoto et al. 2010)
VivoTag 680	820				688		– (Swirski et al. 2007)
YFP	960	228			527		*

[a]: calculated from the σ_2 and φ values

[b]: data from commercial provider

*: data from http://www.drbio.cornell.edu/cross_sections.html (accessed 10/24/2017)

Table 3

Biophysical properties of two-photon–suitable probes specific of brain cells and structures: peak wavelength of two-photon action cross-section (λ_{2PA}) ; peak two-photon action cross-section ($\sigma_2\varphi$) ; peak wavelength of molecular brightness ($\lambda_{\varepsilon\_max}$) ; peak molecular brightness (ε_{max}) ; fluorescence wavelength (λ_{fluo}). Probes discussed in the text are in bold.

Probe	λ_{2PA}[nm]	$\sigma_2\varphi$ [GM]	$\lambda\varepsilon_{max}$ [nm]	ε_{max} [kcpsm]	λ_{fluo} [nm]	Comment	Reference
Alexa Fluor 633			820	~24	647[b]	Arteries (Shen et al. 2012)	Figure 2 in (Mütze et al. 2012)
Ant2-PHEA (in water)	800	490			654	Endothelium	Figure 6 in (Mettra et al. 2016)
Sulforhodamine 101	910	118	900	38.4	~605[b]	Astroglia (Nimmerjahn et al. 2004)	Figure 5 in (Mütze et al. 2012)
Sulforhodamine B	810				~586[b]	Astroglia	Figure 2A in (Appaix et al. 2012)

[a]: calculated from the σ_2 and φ values

[b]: data from commercial provider

Table 4

Biophysical properties of two-photon–suitable environment sensing probes: peak wavelength of two-photon action cross-section (λ_{2PA}) ; peak two-photon action cross-section ($\sigma_2\varphi$) ; fluorescence wavelength (λ_{fluo}). Probes discussed in the text are in bold.

Probe	**λ_{2PA} [nm]**	**$\sigma_2\varphi$ [GM]**	**λ_{fluo} [nm]**	**Comment**	**Reference**
— Chen 2017 Probe L1 (pH 6.73 / pH 4.33)	730	135 / 68a	460 / 580	Ratiometric pH indicator	Figure 6A in (Chen et al. 2017)
— Chen 2017 Probe L2 (pH 5.53 / pH 2.99)	700	67 / 110[a]	465 / 540	Ratiometric pH indicator	Figure 6B in (Chen et al. 2017)
C-Laurdan (in EtOH)	780 (820)	64.5[a]	487	Mechanical strain in the cell membrane	Figure S7 in (Kim et al. 2007)
Laurdan (in EtOH)	780	60[a]	494	Mechanical strain in the cell membrane	Figure S7 in (Kim et al. 2007)
NP1 (in DMF)	740	155	400-500 / 600-750	Ratiometric pH indicator	Figure S4 in (Park et al. 2012)
SNARF-1	< 837		580-640[b]	pH indicator between pH 7 and pH 8	Figure 3 in (Bestvater et al. 2002)
Thiophene DiHemiCyanine	740	~1.4 (with high- viscosity)	~590	Viscosity- sensitive dye	Figure 5A in (Baek et al. 2016)

[a]: calculated from the σ_2 and φ values

[b]: data from commercial provider

Table 5

Biophysical properties of two-photon–suitable probes in the diseased brain: peak wavelength of two-photon action cross-section (λ_{2PA}) ; peak two-photon action cross-section ($\sigma_2\varphi$) ; fluorescence wavelength (λ_{fluo}). Probes discussed in the text are in bold.

Probe	**λ_{2PA} [nm]**	**$\sigma_2\varphi$ [GM]**	**λ_{fluo} [nm]**	**Comment**	**Reference**
Calcofluor White	590		430[b]	Cellulose and chitin binding (identification of fungi and yeast)	Figure 5B in (Trägårdh et al. 2015)
DCIP-1 (in PBS / bound to amyloid- β aggregates)	900	118	675 / 635	Amyloid-β plaques, penetrates BBB	Figure S7 in (Zhu et al. 2017)
Gatifloxacin	700		~510	Fluoroquinolone antibiotics	Figure 1A in (Lee et al. 2016)
MeO-X04 (in PBS / EtOH)	720	10 / 75	452 / 444	Amyloid-β plaques (Klunk et al. 2002)	– (Table S1) (Heo et al. 2013)
MNAH	820		536	Imaging of mitochondrial singlet oxygen	– (Liu et al. 2016)
Moxifloxacin	700		~530	Fluoroquinolone antibiotics	Figure 1A in (Lee et al. 2016)
PIB (in PBS / EtOH)	740	45 / 40	431 / 417	Amyloid-β plaques	– (Table S1) (Heo et al. 2013)
SAD1 (in PBS / EtOH)	750	10 / 170	497 / 465	Amyloid-β plaques	– (Table S1) (Heo et al. 2013)

[a]: calculated from the σ_2 and φ values

[b]: data from commercial provider

Table 6

Biophysical properties of two-photon–suitable functional probes : peak wavelength of two-photon action cross-section (λ_{2PA}) ; peak two-photon action cross-section ($\sigma_2\varphi$) ; peak wavelength of molecular brightness ($\lambda_{\varepsilon\_max}$) ; peak molecular brightness (ε_{max}) ; fluorescence wavelength (λ_{fluo}). Probes discussed in the text are in bold.

Probe	λ_{2PA} [nm]	$\sigma_2\varphi$ [GM]	λ_{ε} max [nm]	ε_{max} [kcpsm]	λ_{fluo} [nm]	Comment	Reference
Calcium indicators							
ACa1 (−Ca^{2+} / +Ca^{2+})	– / 780	– / 110			498 / 498		Figure 2A in (Kim et al. 2008a)
ACa2 (−Ca^{2+} / +Ca^{2+})	– / 780	– / 90			495 / 495		Figure 2A in (Kim et al. 2008a)
ACa3 (−Ca^{2+} / +Ca^{2+})	– / 780	– / 95			500 / 517		Figure 2A in (Kim et al. 2008a)
ACaL (−Ca^{2+} / +Ca^{2+})	– / 780	– / 90			500 / 502		Figure 1B in (Mohan et al. 2009)
ACaLN (−Ca^{2+} / +Ca^{2+})	– / 750	– / 20			494 / 497		– (Table 1) (Lim et al. 2011a)
BCaM (−Ca^{2+} / +Ca^{2+})	– / 780	– / 150			470 / 470		Figure 1C in (Kim et al. 2010a)
Cal-590	1050				590		Figure 1B in (Tischbirek et al. 2015)
Calcium Crimson (+Ca^{2+})	870	95			615[b]		*
Calcium Green (+Ca^{2+})	820, 960	46, 57			531[b]		*
Calcium Orange (+Ca^{2+})	820	60			576[b]		*
CaRuby-Cl	912				604		Figure 5 in (Collot et al. 2012)
CaRuby-F	917				604		Figure 5 in (Collot et al. 2012)
CaRuby-Me	917				604		Figure 5 in (Collot et al. 2012)
Fluo-3	810	13			520-530 (Svoboda and Yasuda 2006)		*
Fluo-4	810		800, 930	~6, ~6	520-530 (Yasuda et al. 2004)		Figure 4 in (Mütze et al. 2012)
Fluo-4FF	810				516[b]		– (Yasuda et al. 2004)
Fluo-5F	810				516[b]		– (Sabatini et al. 2002)
Fluo-8			930, 1000	~4	514[b]		Figure 4 in (Mütze et al. 2012)
Fura-2 +Ca^{2+})	780	~35			505 (Cahalan et al. 2002)		Figure 1B in (Mohan et al. 2009)

Probe	λ_{2PA} [nm]	$\sigma_2\varphi$ [GM]	λ_e max [nm]	ε_{max} [kcpsm]	λ_{fluo} [nm]	Comment	Reference
GCaMP2			950	~6	511 (Tallini et al. 2006)		Figure 4 in (Mütze et al. 2012)
GCaMP3 (−Ca^{2+} / +Ca^{2+})	980	0.126 / 0.33 *			515 (Chen et al. 2013)		Figure 4I in (Helassa et al. 2015)
GCaMP3bright (−Ca^{2+} / +Ca^{2+})	950	0.02 / 0.7 *			~515	high fluorescence dynamic range	Figure 4I in (Helassa et al. 2015)
GCaMP3fast (−Ca^{2+} / +Ca^{2+})	990	0.014 / 0.2 *			~515	fast Ca2+ response times	Figure 4H in (Helassa et al. 2015)
GCaMP5A (pH 9.5)	~940			9.9	~515		– (Table 3) (Akerboom et al. 2012)
GCaMP5D (pH 9.5)	~940			9.0	~515		– (Table 3) (Akerboom et al. 2012)
GCaMP5G (pH 9.5)	~940			9.3	515 (Chen et al. 2013)		Figure 1D in (Akerboom et al. 2012)
GCaMP6f	~940	~35			515 (Chen et al. 2013)		#
GCaMP6s	940	20			515 (Chen et al. 2013)		Figure 5A in (Dana et al. 2016)
iGluSnFR	~940				~515	Glutamate release	Figure S13 in (Marvin et al. 2013)
Indo-1	730				490 / 405 (Cahalan et al. 2002)		* and Figure 3A in (Wang and Yeh 2012)
jRCaMP1a	~1070	~8			~593	OPO-friendly	Figure 2S1B in (Dana et al. 2016)
jRCaMP1b	~1080	~11			~593	OPO-friendly	Figure 2S1B in (Dana et al. 2016)
jRGECO1a	~1070	~7			~593	OPO-friendly	Figure 2S1B in (Dana et al. 2016)
K-GECO1 (−Ca^{2+} / +Ca^{2+})	~1100	~10			594 / 590		Figure 2C in (Shen et al. 2018)
mApple	1070			7.0	592		– (Table 3) (Akerboom et al. 2013)
mRuby	1060			4.0	590		– (Table 3) (Akerboom et al. 2013)
Oregon Green BAPTA-1	800	24			523		Figure 2A in (Kim et al. 2008a)
RCaMP1a (−Ca^{2+} / +Ca^{2+})	1070 / 1070			– / 5.9	594 / 595		– (Table 3) (Akerboom et al. 2013)

Probe	λ_{2PA} [nm]	$\sigma_2\varphi$ [GM]	λ_e max [nm]	ε_{max} [kcpsm]	λ_{fluo} [nm]	Comment	Reference
RCaMP1c (−Ca^{2+} / +Ca^{2+})	1070 / 1070			– / 7.3	597 / 595		– (Table 3) (Akerboom et al. 2013)
RCaMP1d (−Ca^{2+} / +Ca^{2+})	1070 / 1070			– / 7.7	597.5 / 592.5		– (Table 3) (Akerboom et al. 2013)
RCaMP1f (−Ca^{2+} / +Ca^{2+})	1070 / 1070			– / 8.2	597 / 591.5		Figure 2F in (Akerboom et al. 2013)
RCaMP1h	~1070	~27			595		#
R-GECO1 (−Ca^{2+} / +Ca^{2+})	1065 / 1065			– / 3.8	598 / 588		– (Table 3) (Akerboom et al. 2013)
Other ions							
6-CO2H-ZAP4 (−Zn^{2+} / +Zn^{2+})	<700, >1000	– / 86			527 / 523	Zinc	Figure 2B in (Khan et al. 2014)
ANa1 (+Na^{+})	780	95			500	Sodium	Figure 1C in (Kim et al. 2010b)
Asante NaTRIUM Green-2 (ANG- 2) (−Na^{+} / +Na^{+})	780	0.84 / 5.7			542	Sodium	Figure 2 in (Roder and Hille 2014)
AZn1 (−Zn^{2+} / +Zn^{2+})	– / 780	– / 95			496 / 498	Zinc	Figure 1B in (Kim et al. 2008b)
AZn2 (−Zn^{2+} / +Zn^{2+})	– / 780	– / 110			494 / 499	Zinc	Figure 1B in (Kim et al. 2008b)
AZnE1 (−Zn^{2+} / +Zn^{2+})	– / 780	– / 86			502 / 503	Zinc	Figure 2A in (Danish et al. 2011)
AZnE2 (−Zn^{2+} / +Zn^{2+})	– / 780	– / 86			503 / 504	Zinc	Figure 2A in (Danish et al. 2011)
AZnM1 (−Zn^{2+} / +Zn^{2+})	– / 780	– / 88			501 / 504	Zinc	Figure 2A in (Danish et al. 2011)
AZnM2 (−Zn^{2+} / +Zn^{2+})	– / 780	– / 86			504 / 504	Zinc	Figure 2A in (Danish et al. 2011)
AZnN (−Zn^{2+} / +Zn^{2+})	– / 780	– / 89			500 / 502	Zinc	Figure 2A in (Danish et al. 2011)
FMg1 (−Mg^{2+} / +Mg^{2+})	– / 740	– / 87			540 / 540	Magnesium	Figure 1C in (Dong et al. 2012)
FMg2 (−Mg^{2+} / +Mg^{2+})	– / 740	– / 76			555 / 555	Magnesium	Figure 1C in (Dong et al. 2012)
NC7	860	77[a]			520	Magnesium	Figure 4 in (Yin et al. 2015)
OC7	740	71[a]			500	Magnesium	Figure 4 in (Yin et al. 2015)
PhenGreen-FL	1074				517 (Petrat et al. 1999)	Heavy metals	Figure 3 in (Bestvater et al. 2002)
P-Zn (−Zn^{2+} / +Zn^{2+})	700 / 700	304 / 565[a]			465 / 550	Zinc	Figure 1A in (Li et al. 2017)
SBFI (+Na^{+})	780	20			539	Sodium	Figure 1C in (Kim et al. 2010b)
Sodium Green(+Na^{+})	800	30			532	Sodium	Figure 1C in (Kim et al. 2010b)

Brain Struct Funct. Author manuscript; available in PMC 2019 September 01.

Probe	λ_{2PA} [nm]	$\sigma_{2\varphi}$ [GM]	λ_{e} max [nm]	ε_{max} [kcpsm]	λ_{fluo} [nm]	Comment	Reference
SZn-Mito (−Zn^{2+} / +Zn^{2+})	– / 760	– / 75			500 / 493	Zinc	Figure 1B in (Masanta et al. 2011)
SZn2-Mito (−Zn^{2+} / +Zn^{2+})	– / 750	– / 155			536 / 536	Zinc	Figure 1B in (Baek et al. 2012)
SZnC (−Zn^{2+} / +Zn^{2+})	750 / 750	16 / 92			499 / 499	Zinc (Golgi- localized)	Figure 2D in (Singh et al. 2015)
— Schwarze 2015 Probe 1 (DMSO / K^{+} / Na^{+})	860	3.1 / 9.4 / 3.4			511	Potassium / Sodium	Figure 2B in (Schwarze et al. 2015)
— Schwarze 2015 Probe 2 (DMSO / K^{+})	840	5.7 / 16.1			493	Potassium	– (Table 1) (Schwarze et al. 2015)
Voltage-sensitive dyes							
ANNINE-6	1020				560-660 (Frey et al. 2006)		– (Kuhn et al. 2008)
ANNINE-6plus	1060				560-660		– (Kuhn et al. 2004)
ArcLight A242	950				<775		– (Table 1) (Brinks et al. 2015)
ASAP1	950				<775		– (Table 1) (Brinks et al. 2015)
BP6	740	100			545	Mitochondrial membrane potential	Figure 7 in (Moritomo et al. 2014)
CAESR	968				<775		– (Table 1) (Brinks et al. 2015)
di-2- ANEP(F)PTEA	1060				632 (bound to lipids)		– (Yan et al. 2012)
di-3- ANEPPDHQ	850				>560		Figure 5A in (Fisher et al. 2008)
Di-4-ANEPPS	940	5			635 (in ethanol)[b]		*
Di-8- ANEPPDHQ	~900- 950	~20			620 (in octanol)		Figure 3 in (Fisher et al. 2005)
Di-8-ANEPPS	940	10			625 (in octanol)		*and Figure 5 in (Fisher et al. 2005)
FlicR1	1120				597	OPO-friendly	– (Abdelfattah et al. 2016)
Merocyanine 540	>950	4.4 (at 960 nm)			615 (in octanol)		Figure 3 in (Fisher et al. 2005)
Nile Blue A	<800	0.6 (at 800 nm)			660 (in octanol)		Figure 3 in (Fisher et al. 2005)
QuasAr1	1200				660-775		– (Table 1) (Brinks et al. 2015)
QuasAr2	1200				660-775		Figure S3 in (Brinks et al. 2015)
RH-1692	~800- 850	1.5 (at 800 nm)			680 (in octanol)		Figure 3 in (Fisher et al. 2005)

Probe	λ_{2PA} [nm]	$\sigma_2\varphi$ [GM]	λ_{e} max [nm]	ε_{max} [kcpsm]	λ_{fluo} [nm]	Comment	Reference
RH-237	<800, >960	8.9 (at 800 nm)			676 (in octanol)		Figure 3 in (Fisher et al. 2005)
RH-414	~950	12 (at 960 nm)			636 (in octanol)		Figure 3 in (Fisher et al. 2005)
RH-421	~950	16 (at 960 nm)			648 (in octanol)		Figure 3 in (Fisher et al. 2005)
RH-795	~950	10 (at 960 nm)			640 (in octanol)		Figure 3 in (Fisher et al. 2005)

[a]: calculated from the σ_2 and φ values

[b]: data from commercial provider

[*]: data from http://www.drbio.cornell.edu/cross_sections.html (accessed 10/24/2017)

[#]: data from https://www.janelia.org/lab/harris-lab-apig/research/photophysics/two-photon-fluorescent-probes (accessed 10/24/2017)

Table 7

Biophysical two-photon properties of intrinsic fluorophores : peak wavelength of two-photon action cross-section (φ_{2PA}) ; peak two-photon action cross-section ($\sigma_2\varphi$) ; peak wavelength of molecular brightness ($\varphi_{\varepsilon\_max}$) ; peak molecular brightness (ε_{max}) ; fluorescence wavelength (φ_{fluo}). Probes discussed in the text are in bold.

Probe	φ_{2PA} [nm]	$\sigma_2\varphi$ [GM]	φ_{fluo} [nm]	Comment	Reference
Cholecalciferol	<700, 820, 980	0.0006 (at 700 nm)	460	Vitamin D3	Figure 1A in (Zipfel et al. 2003a)
FAD	~880	<1	~530		Figure 1B in (Stringari et al. 2017)
Folic acid	<700	0.007 (at 700 nm)	~445	Vitamin B9	Figure 1A in (Zipfel et al. 2003a)
NADH	700	0.09 (at 700 nm)	~470		Figure 1A in (Zipfel et al. 2003a)
Pyridoxine	<700	0.008 (at 700 nm)	~390		Figure 1A in (Zipfel et al. 2003a)
Retinol	<700	0.07 (at 700 nm)	~490		Figure 1A in (Zipfel et al. 2003a)
Riboflavin	<700	0.8 (at 700 nm)	~530		Figure 1A in (Zipfel et al. 2003a)

Table 8

Biophysical properties of two-photon–suitable probes specific of sub-cellular structures : peak wavelength of two-photon action cross-section (φ_{2PA}) ; peak two-photon action cross-section ($\sigma_2\varphi$) ; peak wavelength of molecular brightness ($\varphi_{\varepsilon\_max}$) ; peak molecular brightness (ε_{max}) ; fluorescence wavelength (φ_{fluo}). Probes discussed in the text are in bold.

Probe	**φ_{2PA} [nm]**	**$\sigma_2\varphi$ [GM]**	**λ_{fluo} [nm]**	**Comment**	**Reference**
Acridine Orange	837 > 882 >> 981		526 (DNA), 650 (RNA)[b]	Nucleic acids	Figure 3 in (Bestvater et al. 2002)
ANO1	750	170	502	Nitric oxide	Figure 3 in (Seo et al. 2012)
AS1	780	85	498	Glucose	Figure S6A in (Lim et al. 2012)
ASiR1 (in CH_3CN)	750	258	593	Lysosomes	Figure S2 in (Zhang et al. 2018)
ASiR2 (in CH_3CN)	760	237	601	Lysosomes	Figure S2 in (Zhang et al. 2018)
ASiR3 (in CH_3CN)	760	160	606	Lysosomes	Figure S2 in (Zhang et al. 2018)
ASiR4 (in CH_3CN)	760	179	608	Lysosomes	Figure S2 in (Zhang et al. 2018)
ASiR5 (in CH_3CN)	750	189	609	Lysosomes	Figure S2 in (Zhang et al. 2018)
ASiR6 (in CH_3CN)	750	193	601	Lysosomes	Figure S2 in (Zhang et al. 2018)
ASS (H_20 / 2- AET)	780	11 / 113	457 / ~505	Thiols	Figure 1D in (Lee et al. 2010)
BLT-blue	750	160	451	Lysosomes	Figure 1B in (Han et al. 2012)
CAEI	850	152	550	Mitochondria	Figure 1B in (Miao et al. 2014)
CAI	860	328	562	Mitochondria	Figure 1B in (Miao et al. 2014)
CLT-blue	750	50	471	Lysosomes	Figure 1B in (Son et al. 2011)
CLT-yellow	850	47	549	Lysosomes	Figure 1B in (Son et al. 2011)
C-Laurdan (in EtOH)	780	64.5[a]	487	Lipid rafts	Figure S7 in (Kim et al. 2007)
DAPI	580 >> 685		461[b]	Nucleic acids	Figure 2A in (Trägårdh et al. 2015)
DCF2 (H_2DCFDA) (in DMSO)	1065		538 (Yi et al. 2009)	Organelle tracker	Figure 3 in (Bestvater et al. 2002)
DiA	880 (study limited to [830-920 nm])		590	Lipophilic Tracer	– (Table 1) (Ruthazer and Cline 2002)
DiD	830		665	Lipophilic Tracer	– (Table 1) (Ruthazer and Cline 2002)
DiI	<700, 1020	96, 10	565 (Cahalan et al. 2002)	Lipophilic Tracer, organelles	*

Probe	φ_{2PA} [nm]	$\sigma_2\varphi$ [GM]	λ_{fluo} [nm]	Comment	Reference
DiO	880 (study limited to [830-920 nm])		501	Lipophilic Tracer	– (Table 1) (Ruthazer and Cline 2002)
ER-Tracker white/blue	728		430-640[b]	Endoplasmic Reticulum (environmentally- sensitive)	Figure 5 in (Bestvater et al. 2002)
FMT-green	750	175	523	Mitochondria	Figure 1B in (Han et al. 2012)
Hoechst 33258	560 >> 717		461[b]	Nucleic acids	Figure 5A in (Trägårdh et al. 2015)
Hoechst 33342	660 > 715		461[b]	Nucleic acids	Figure 3A in (Bestvater et al. 2002)
Laurdan (in EtOH)	780	60[a]	494	Lipid rafts	Figure S7 in (Kim et al. 2007)
LysoTracker Red	1010 < 1100		590[b]	Organelle tracker	Figure 5 in (Bestvater et al. 2002)
LysoTracker Yellow	972		535[b]	Organelle tracker	Figure 5 in (Bestvater et al. 2002)
MitoTracker Red	860, 1133	3.12 (at 860 nm)	599[b]	Organelle tracker	Figure 5 in (Bestvater et al. 2002)
PKH26	950		567[b]	Membrane labelling	– (Takaki et al. 2015)
PKH67	870, 850		502[b]	Membrane labelling	– (Morelli et al. 2003; Kuwashima et al. 2005)
Propidium iodide	989 > 1015 >> 1099		617[b]	Nucleic acids (dead cells)	Figure 3 in (Bestvater et al. 2002)
Quinacrine	678 > 697		525[b]	Nucleic acids, therapeutic effect	Figure 3 in (Bestvater et al. 2002)
SL2 (in EtOH / THF)	800	40 / 185	576 / 495	Lipid rafts, turn-on	Figure 1B in (Lim et al. 2011b)
Rhodamine 123	913 > 1090		527[b]	Mitochondria	Figure 3 in (Bestvater et al. 2002)
SYBR Gold	~820		~537[b]	Nucleic acids	Figure 3 in (Neu et al. 2002)
SYBR Green	~820		520[b]	Nucleic acids	Figure 3 in (Neu et al. 2002)
Syto 13	~780-800		509 (DNA), 514 (RNA)[b]	Nucleic acids	Figure 2 in (Neu et al. 2002)
Syto 40	900		441[b]	Nucleic acids	Figure 2 in (Neu et al. 2002)
Syto 9	<800		503[b]	Nucleic acids	Figure 2 in (Neu et al. 2002)
Sytox Blue	<800		480[b]	Nucleic acids	Figure 3 in (Neu et al. 2002)
Sytox Green	~715		523[b]	Nucleic acids	Figure 5C in (Trägårdh et al. 2015)
TO-PRO-3	1110		661[b]	Nucleic acids, OPO- friendly	– (Smith et al. 2012)

[a]: calculated from the σ_2 and φ values

b: data from commercial provider

*: data from http://www.drbio.cornell.edu/cross_sections.html (accessed 10/24/2017)